Neutron spectroscopy: vibrational dynamics and tunneling of water in minerals*

A.I. Kolesnikov
Oak Ridge National Laboratory
Oak Ridge, TN

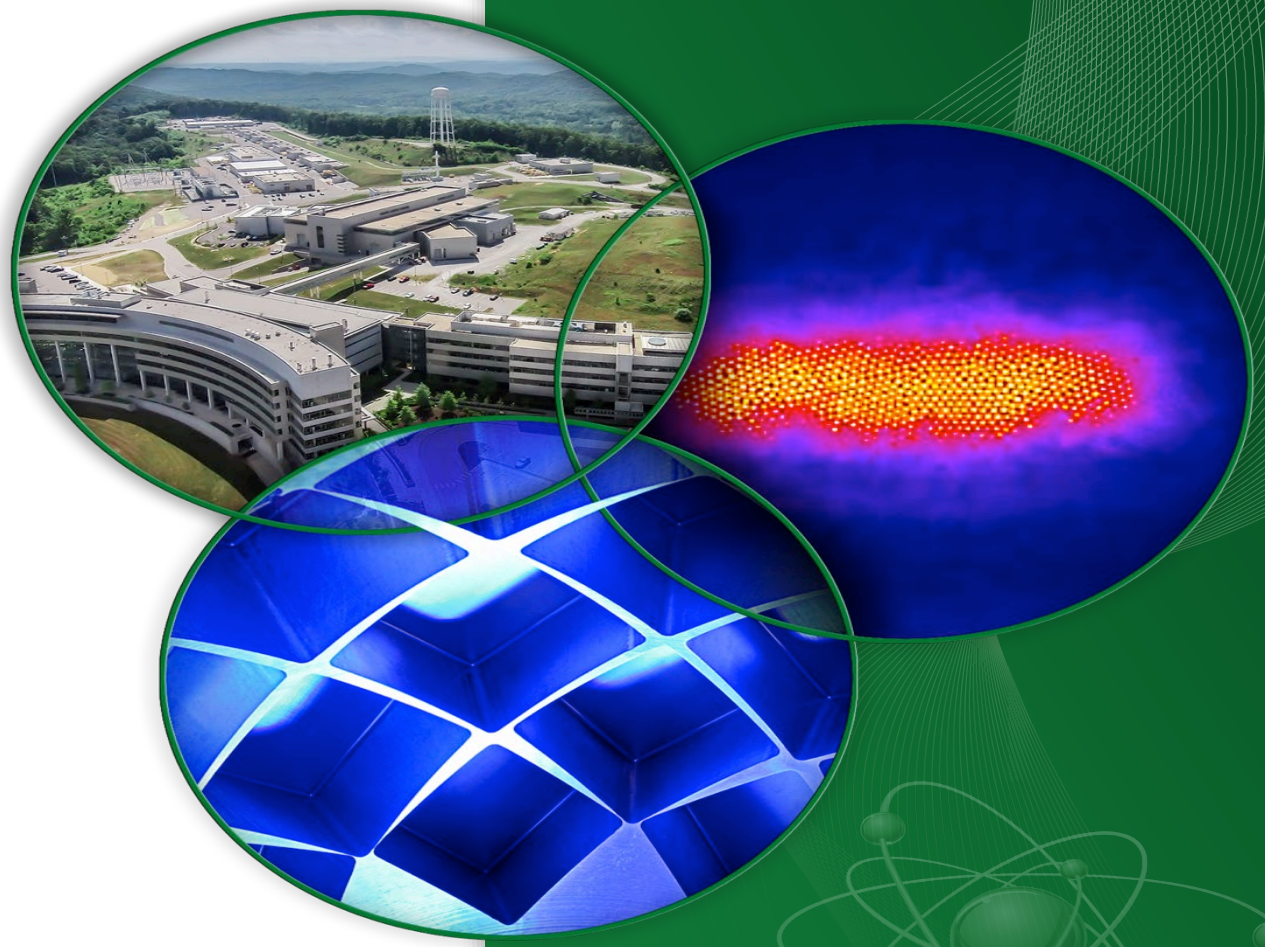

***The neutron experiments at ORNL's Spallation Neutron Source were supported by the Scientific User Facilities Division, Office of Science (Basic Energy Sciences), U.S. Department of Energy (DOE).**

ORNL is managed by UT-Battelle
for the US Department of Energy

OAK RIDGE National Laboratory | SPALLATION NEUTRON SOURCE

OUTLINE

- **Introduction**
- **Fast rotational dynamics of water in hemimorphire**
- **Dynamics of water in beryl**
- **Summary**

Dom Pedro Aquamarine (Beryl) at the Smithsonian's National Museum of Natural History, Washington D.C.

Hemimorphite, Ojuela Mine, Mapimi, Durango, Mexico

SNS, ORNL

SEQUOIA: The Fine Resolution Fermi Chopper Spectrometer

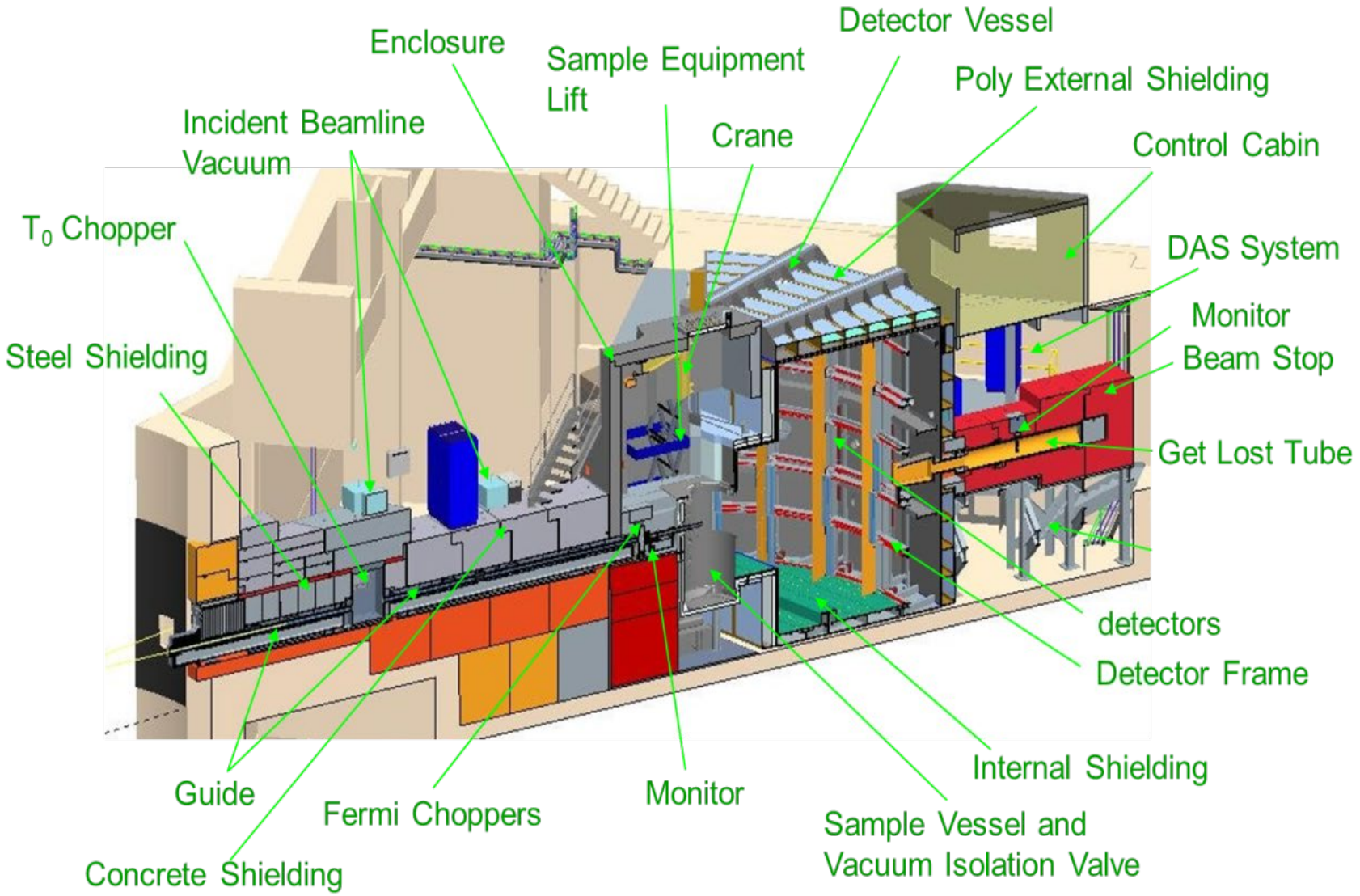

E_i = 4 − 6000 meV
Scattering angles:
-30 to 60° (h), ±18° (v)

Examples of different bulk and confined water

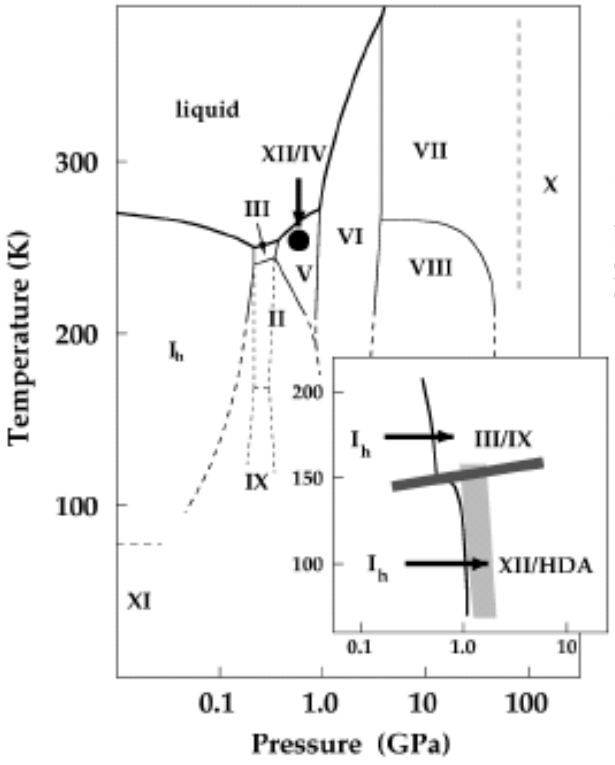

Phase diagram of ice

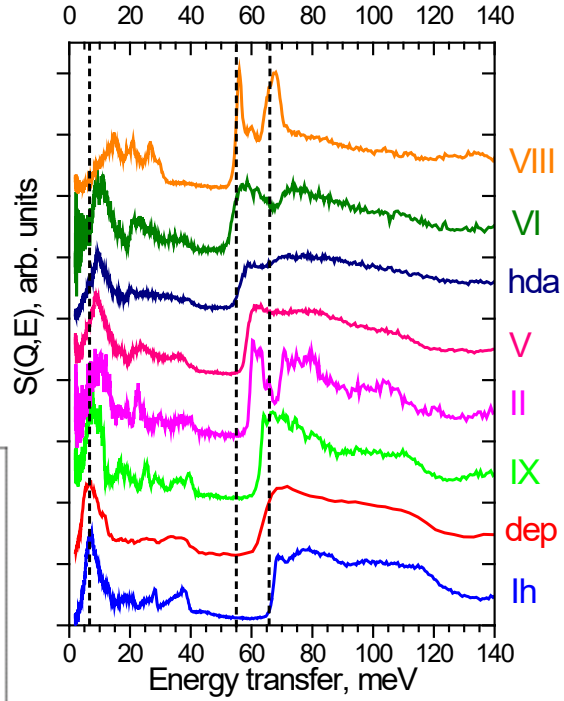

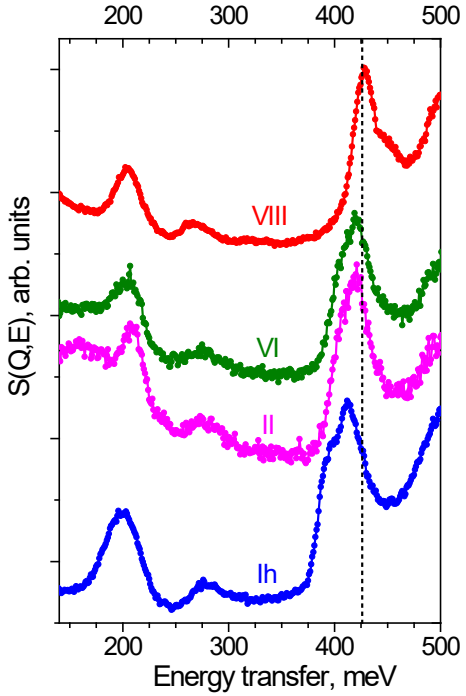

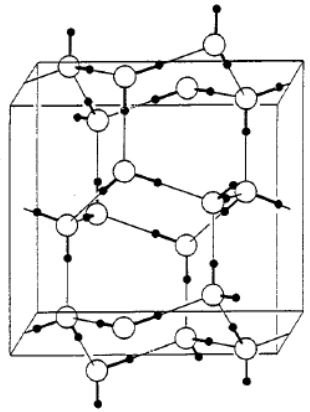

Ice-Ih

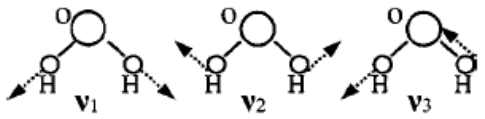

Schematic illustration of the bending and stretching modes in water molecule.

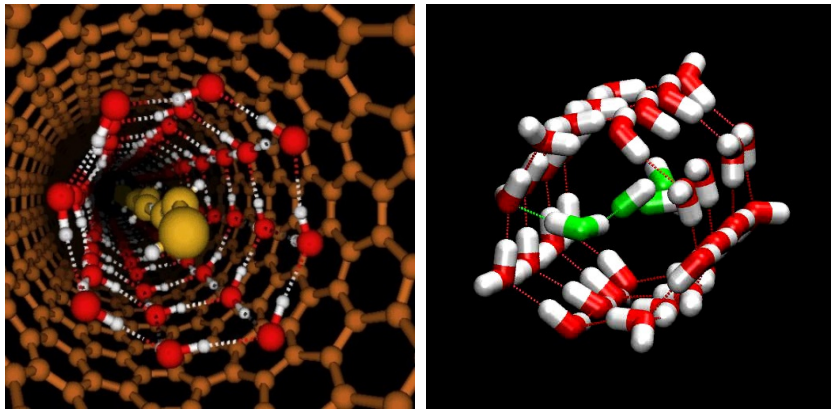

Water in SWNT

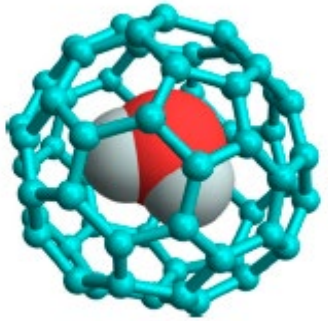

H_2O water in fullerene C_{60}
Beduz et al.
PNAS, 2012

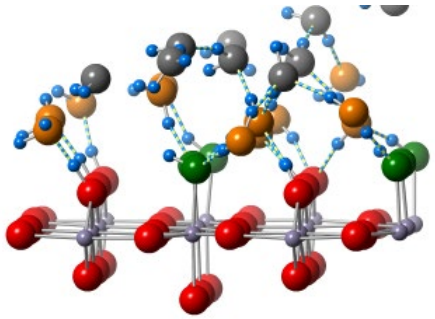

Water on surface of cassiterite (SnO_2)

OUTLINE

- Introduction
- **Fast rotational dynamics of water in hemimorphire**
- Dynamics of water in beryl
- Summary

Dom Pedro Aquamarine (Beryl) at the Smithsonian's National Museum of Natural History, Washington D.C.

Hemimorphite, Ojuela Mine, Mapimi, Durango, Mexico

Hemimorphite, $Zn_4Si_2O_7(OH)_2 \cdot H_2O$

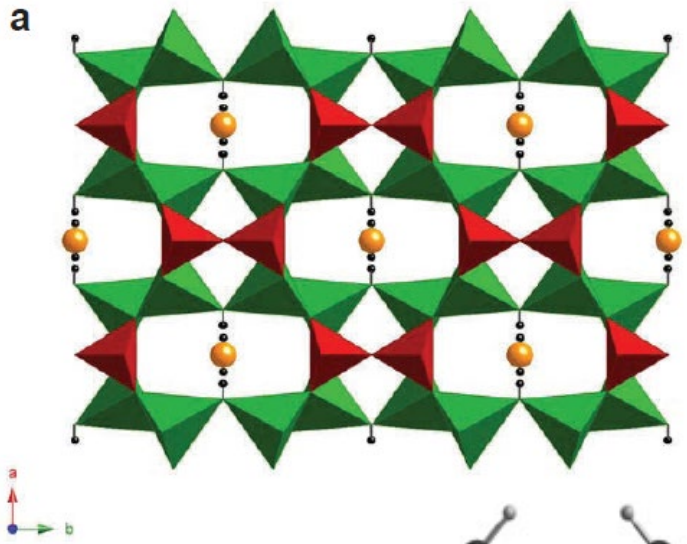

(a) Hemimorphite structure at 300 K (*Imm2)*. The green tetrahedra − $ZnO_3(OH)$ groups, and the red − SiO_4 groups. The orange spheres are the O atoms of the H_2O molecules and the small black points are H atoms.
C.A. Geiger & E. Dachs
Am. Mineral. 94 (2009) 634

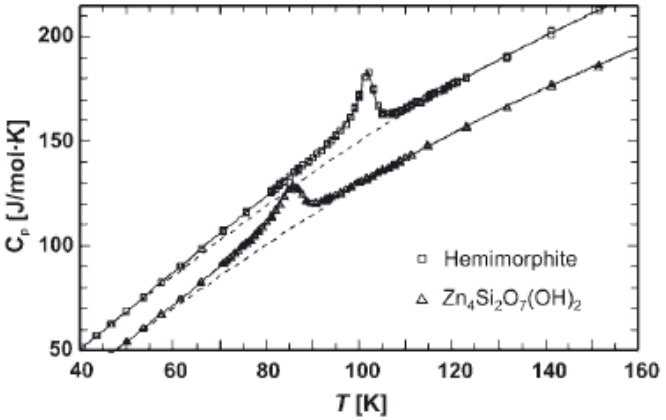

Fig. 5. Experimental heat capacity for hemimorphite (squares) and $Zn_4Si_2O_7(OH)_2$ (triangles) in the temperature region of their respective phase transitions. Interpolated heat capacity (dashed lines) is based on Equation (1). It is obtained by modelling heat-capacity behaviour outside the transitions with Debye, Einstein and Schottky functions (*DES* + *spline* approach). The solid line is the sum $C_p^{eq.(1)} + \Delta C_p$, *i.e.* the sum of the *DES*-fit + cubic *spline* fit to ΔC_p.

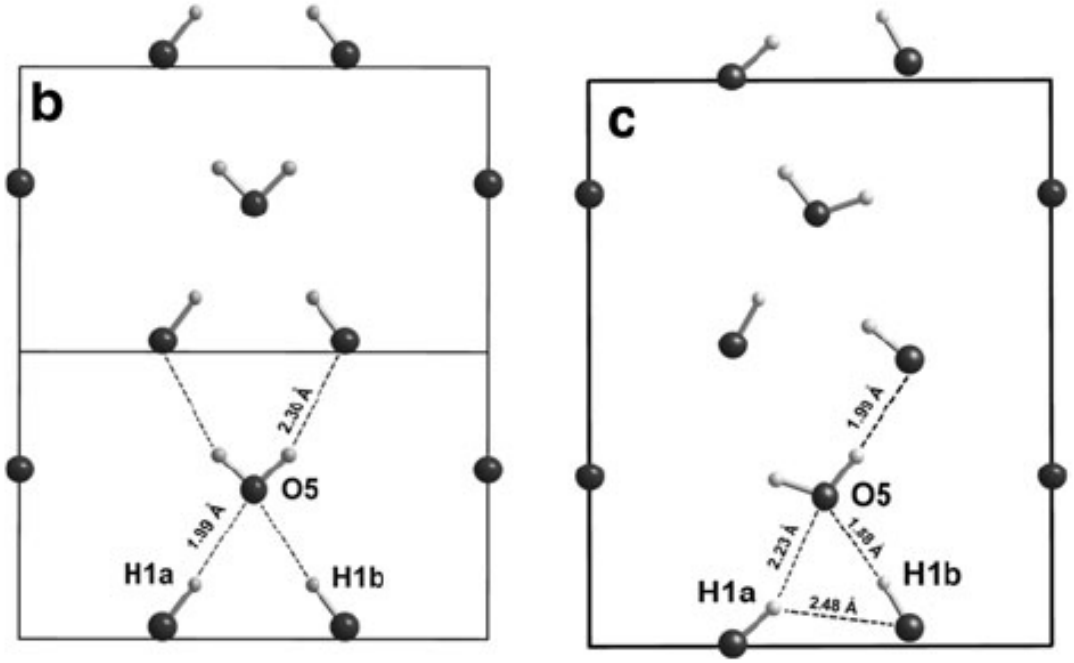

Comparison of the positions and orientations of the water molecule and the hydroxyl groups in the (010) plane at RT (Imm2) and 20 K (*Abm2).*
(b) Hill *et al., Z Kristallogr*. 146 (1977) 241
(c) Libowizky *et al., Z Kristallogr.* 213 (1998) 659

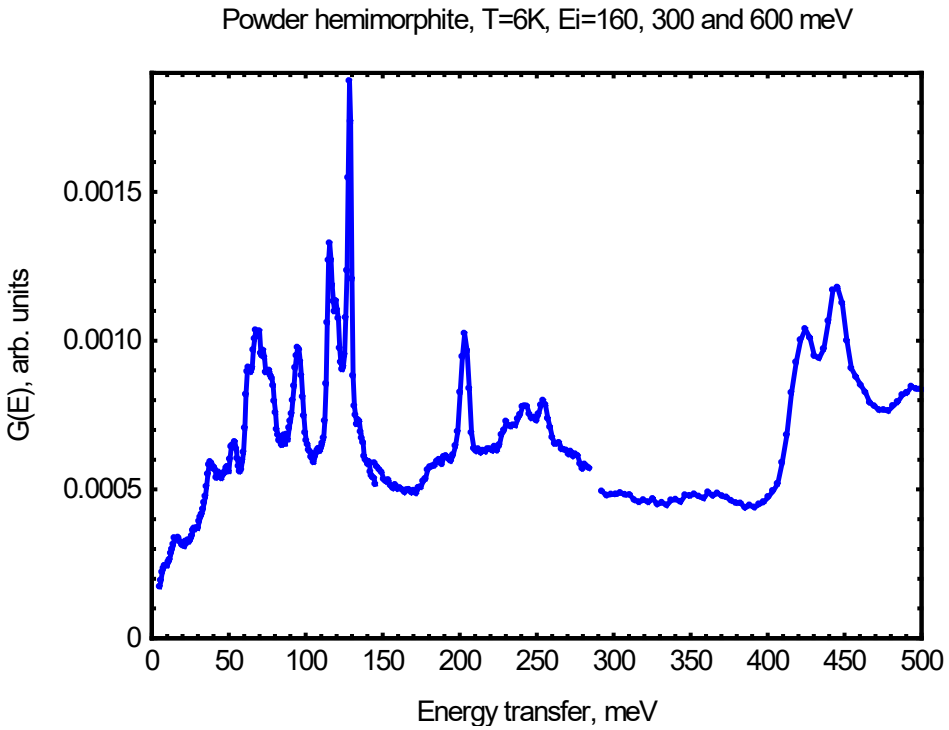

INS spectra of powder hemimorphite measured at SEQUOIA at T=6K with Ei=160, 300 and 600 meV.

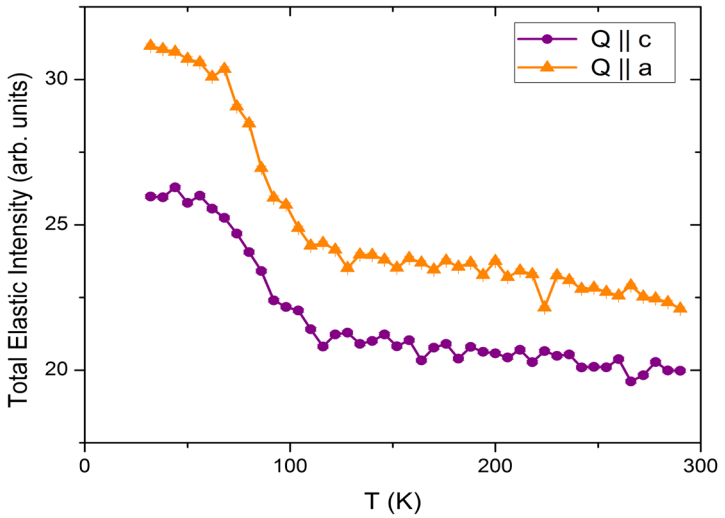

BASIS representative fixed window scans obtained in two different orientations of the hemimorphite crystals.

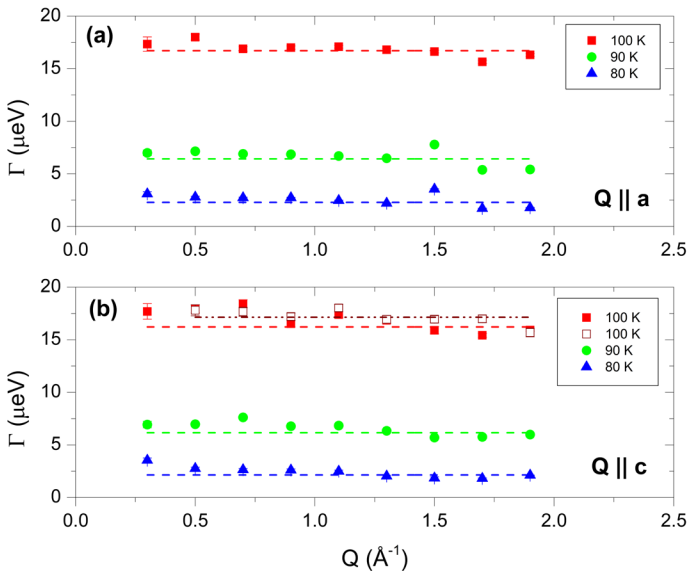

The intrinsic half-width at half-maximum Γ of the Lorentzian component observed at BASIS. At each temperature, the points are fitted to a horizontal line.

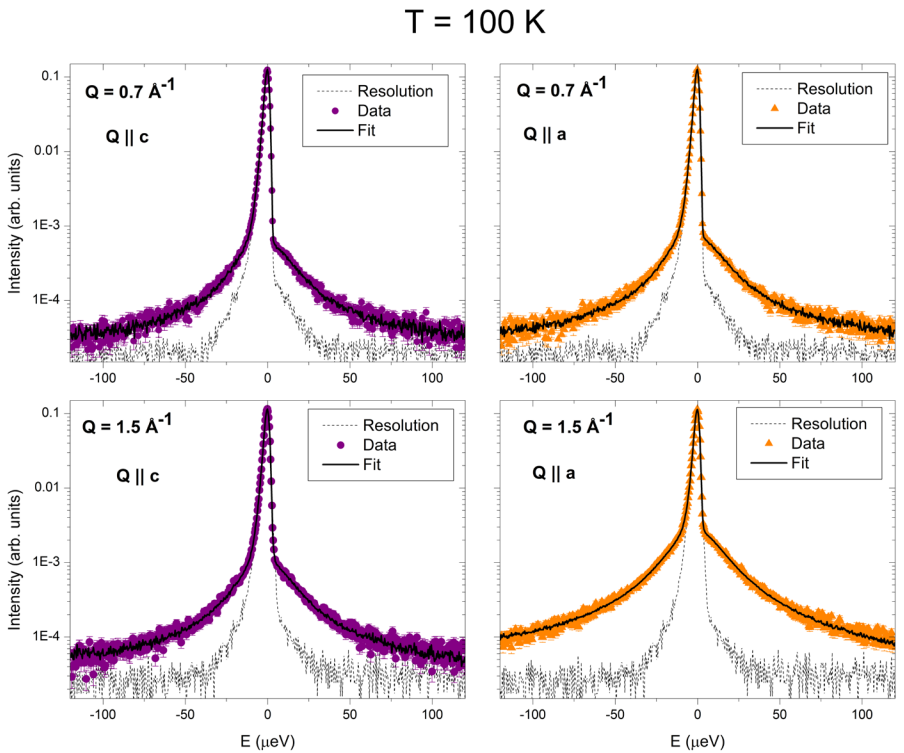

Representative BASIS QENS data of hemimorphite fitted with 1 Lorentzian function for Q||c and Q||a configurations.

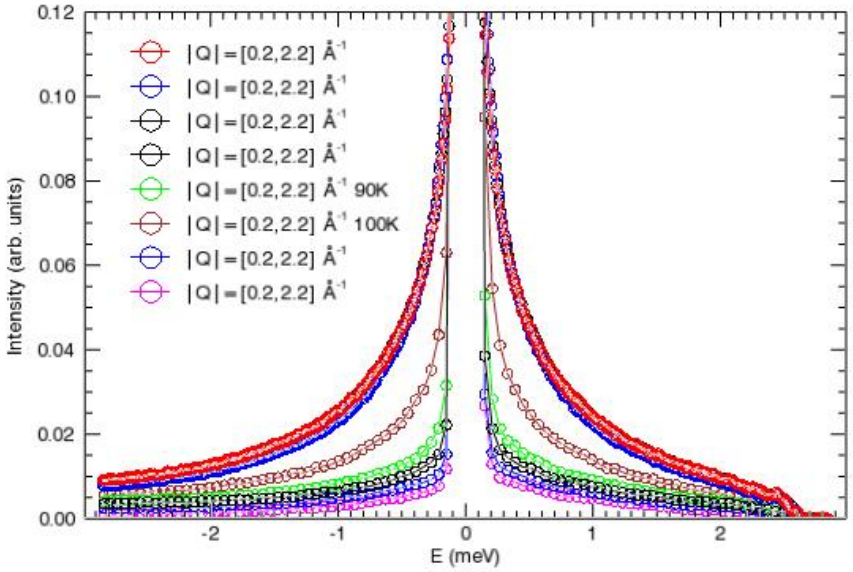

INS spectra of hemimorphite obtained with CNCS using E_i= 3 meV and 12 meV.

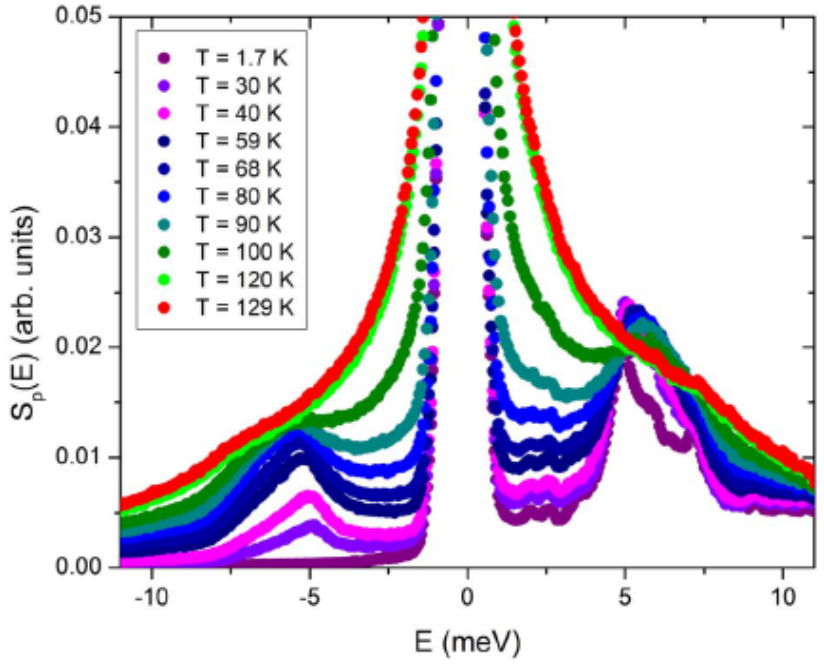

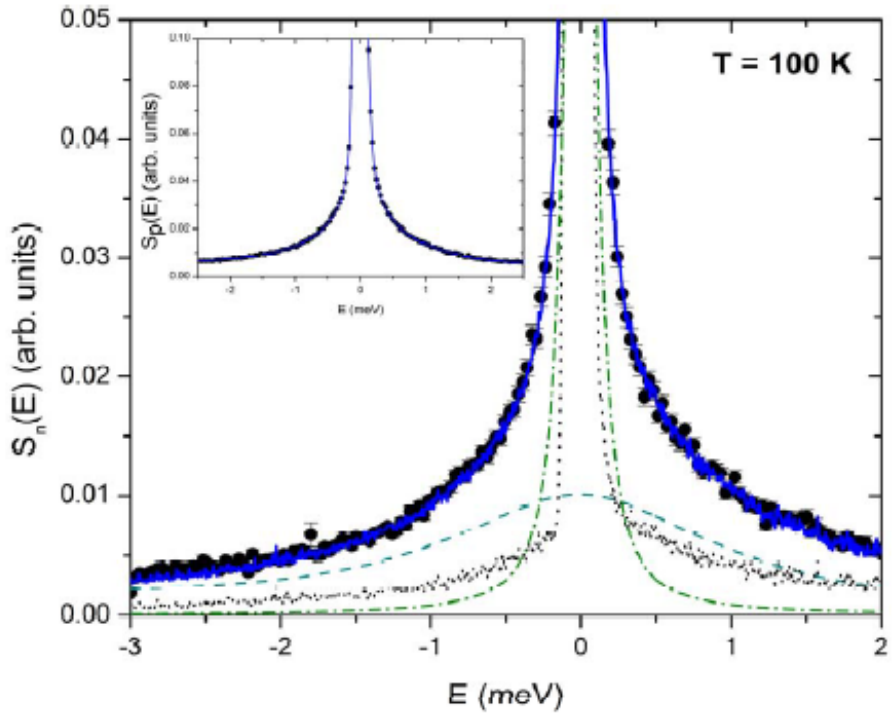

$$\mathbf{S(E)} = \boldsymbol{A_0}\delta(\boldsymbol{E}) + \sum_{\boldsymbol{i=1}}^{\boldsymbol{2}} \frac{\boldsymbol{A_i}}{\boldsymbol{\pi}} \frac{\boldsymbol{\Gamma_i}}{\boldsymbol{\Gamma_i^2 + E^2}} + \boldsymbol{C_1 E} + \boldsymbol{C_2}$$

Representative CNCS QENS spectra fitted with 2 Lorentzian functions for Q||c (main) and Q||b (insert) configurations.

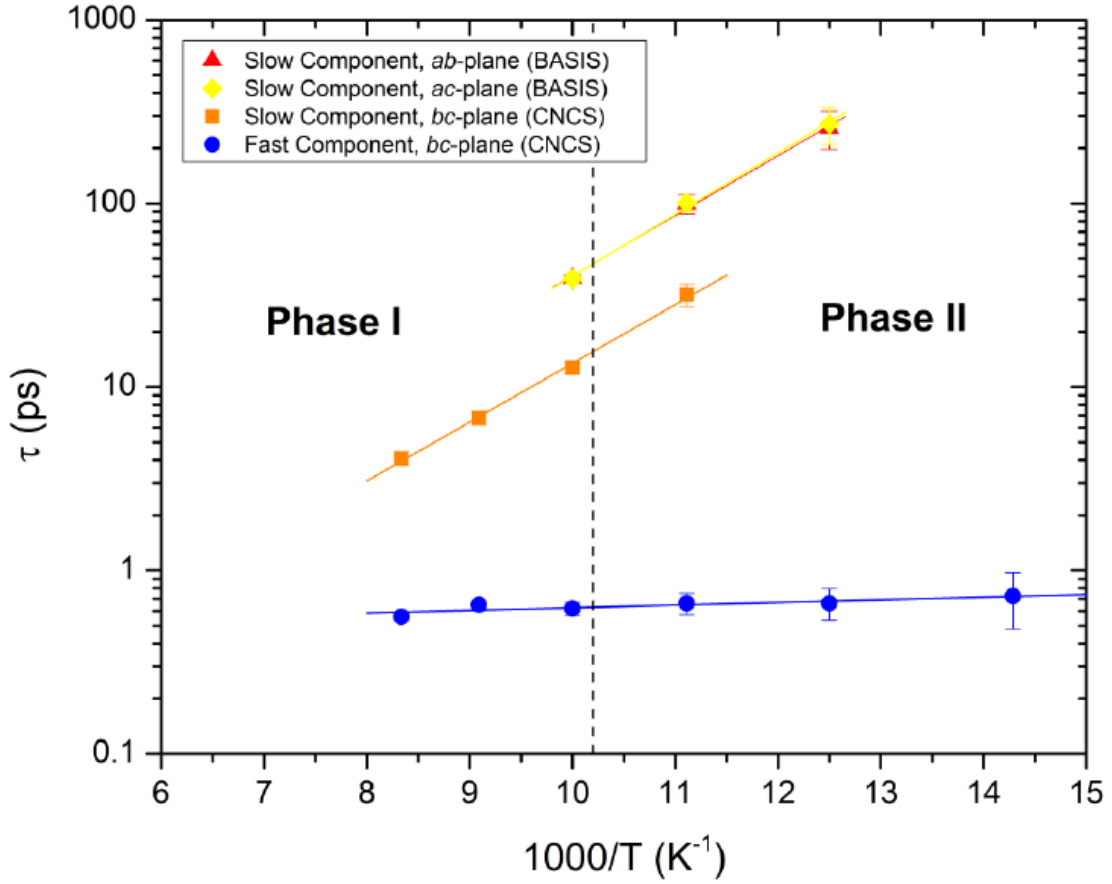

Arrhenius plot of the relaxation times, $\tau = \hbar/\Gamma$, obtained from QENS data; the lines are fit to $\tau(T) = \tau_0 e^{E_a/k_B T}$.

Two types of localized diffusion are observed between 70 K ≤ *T* ≤ 120 K.

First, a slow process with a relaxation time 10-100 ps, involves the breaking of HB, E_a=6.6±0.4 kJ/mol (or 68±4 meV).

Second, a faster process with a relaxation time <1 ps, does not involve the breaking of HB, E_a=0.4±0.2 kJ/mol (or 4±2 meV).

The breaking of HB in bulk liquid water obeys an Arrhenius law with an activation energy of 10 kJ=mol (Conde&Teixeira, J. Phys. 44 (1983) 525; Montrose et al., J. Chem. Phys. 60 (1974) 5025).

TOPAZ, SNS

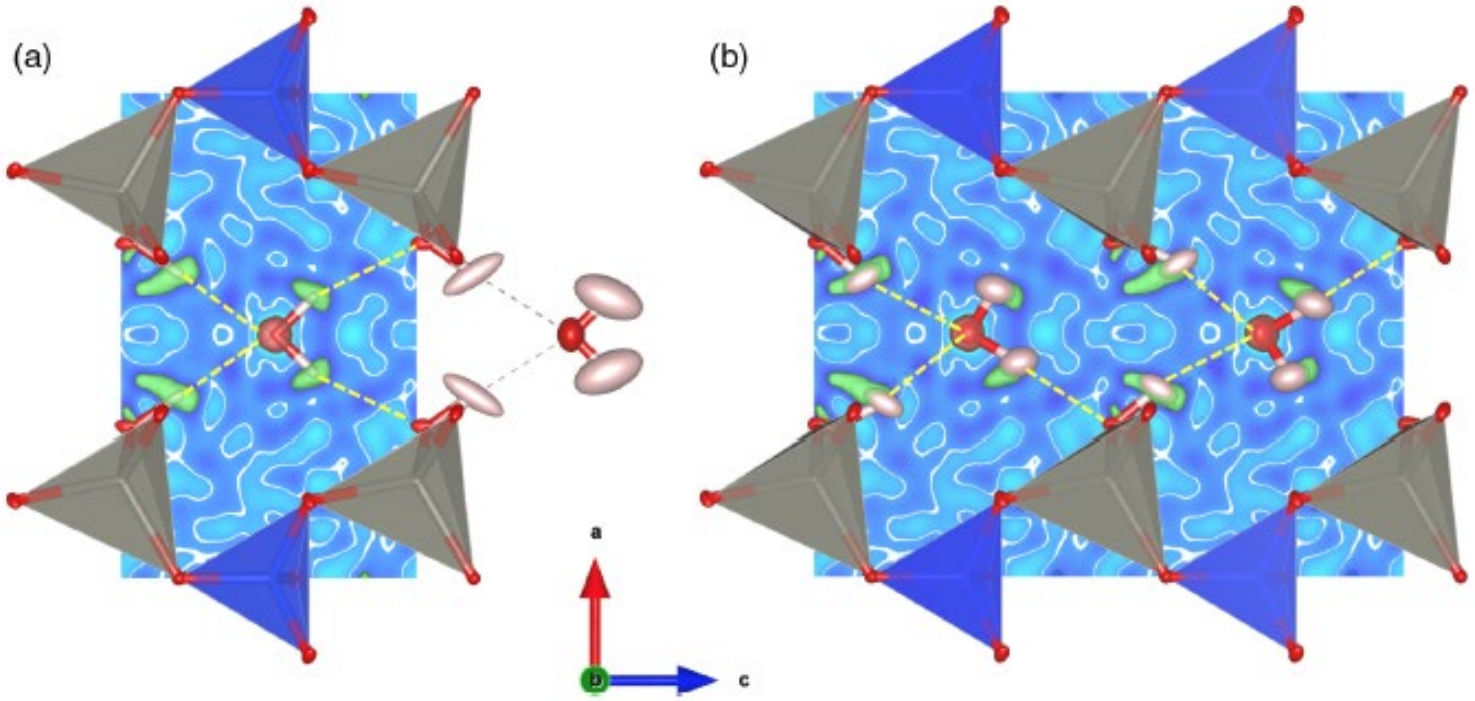

The crystal structure of hemimorphite. The framework is shown as a ball-and-stick model with anisotropic displacement parameters at 65% probability. The hydroxyl proton and the water molecule are shown as nuclear density isosurfaces.

Panel (a) illustrates model A for phase I at T=110 K, and panel (b) illustrates the unit cell for phase II at T=90 K. Model B for phase I is the same as shown on panel (b) with random occupancy of the water molecules.

Model A provides an isotropic $\langle u^2_{iso} \rangle$ = 0.08 Å^2, and model B gives $\langle u^2_{iso} \rangle$ = 0.02 Å^2. Figure designations: Nuclear density isosurfaces for water oxygens (red), nuclear density isosurfaces for water or hydroxyl protons (green), SiO_4 tetrahedra (blue), $ZnO_3(OH)$ tetrahedra (gray), framework oxygen (red).

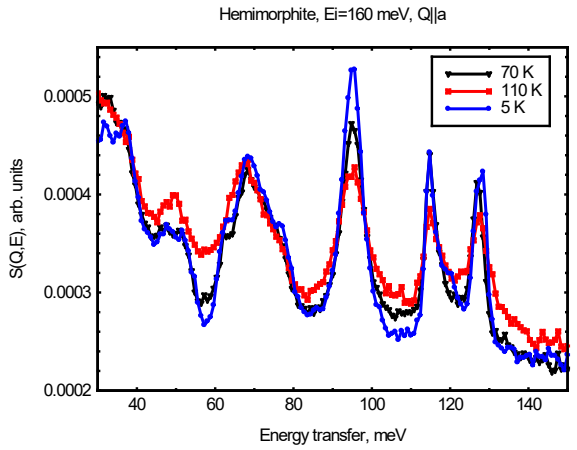

If the large value of $\langle u^2_{iso} \rangle$=0.08 Å^2 of Model A represents the dynamical displacements of the water hydrogens, then the water vibrational modes would likely not be observable in INS data due to strong suppression by the Debye-Waller factor.

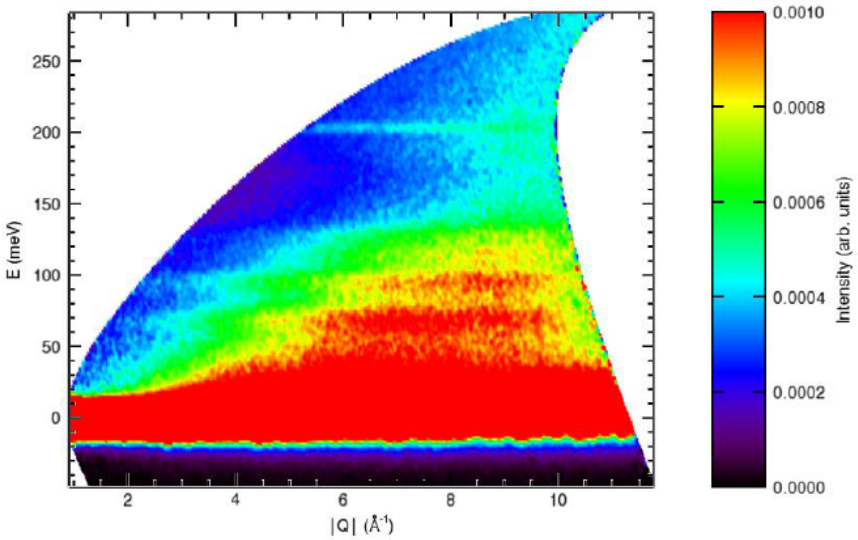

Figure 9. A slice of the dynamic structure factor $S(\mathbf{Q}, E)$ obtained using the SEQUIOA spectrometer for $\mathbf{Q} \parallel a$ at 110 K. The constant band around 200 meV is the water scissors mode ν_2.

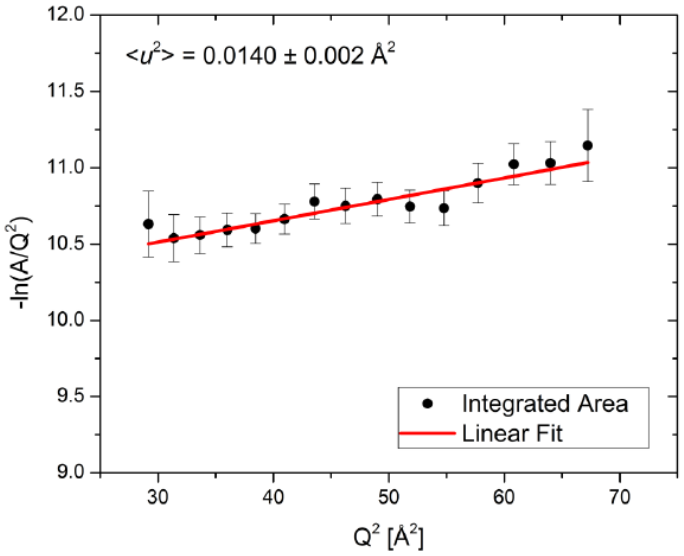

Figure 10. The integrated intensity $A(Q)$ of the water scissors mode ν_2 at 110 K. The slope estimates the dynamic mean-squared displacement $\langle u^2 \rangle$ of the water hydrogens.

The $\langle u^2 \rangle$ for water protons estimated from the INS spectra, $S(Q,E) \propto Q^2 exp(-\langle u^2 \rangle Q^2)$, is about 0.014 Å^2, which is close to the value for refinement with the model B, $\langle u^2_{iso} \rangle$ = 0.02 Å^2.

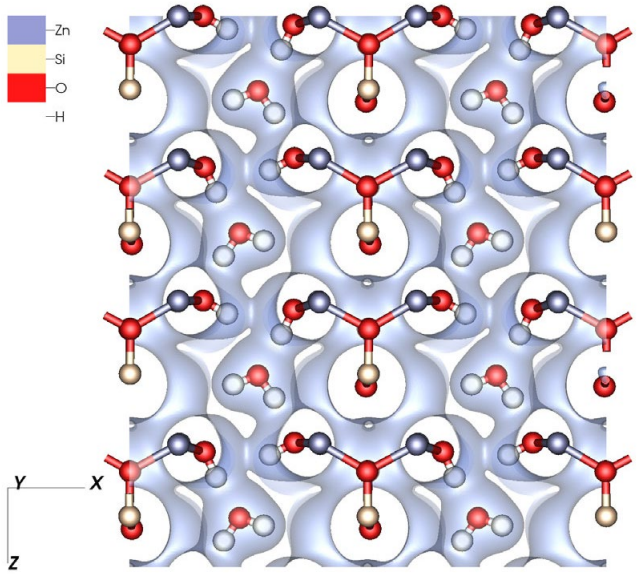

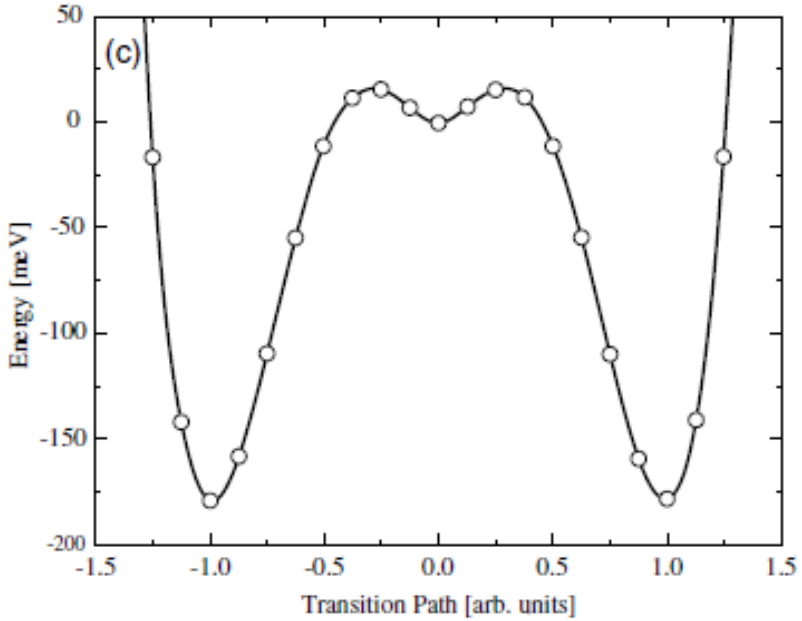

The cross section of the DFT structure and isosurface of the electronic charge density, illustrating the in-plane alternating layout of the water molecules.

The DFT calculations (Paul Kent, ORNL) of a 160-atom hemimorphite supercell {8 × [Zn4Si2O7(OH)2 ·H2O]} containing eight water molecules were performed using the plane wave pseudopotential projector-augmented wave method as implemented in the VASP code. We used the PBE functional and the DFT+D2 van der Waals method.

The calculated orientational potential barrier of eight water molecules obtained from the DFT calculations.

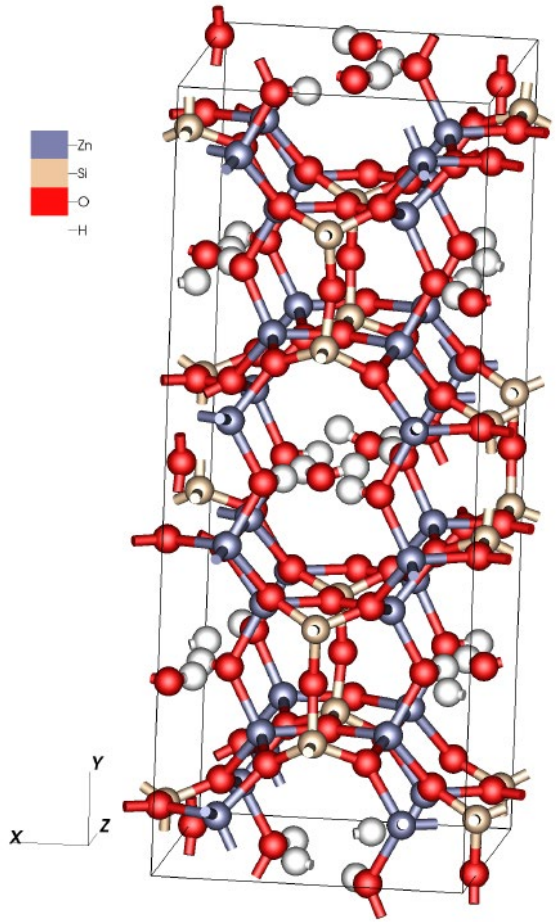

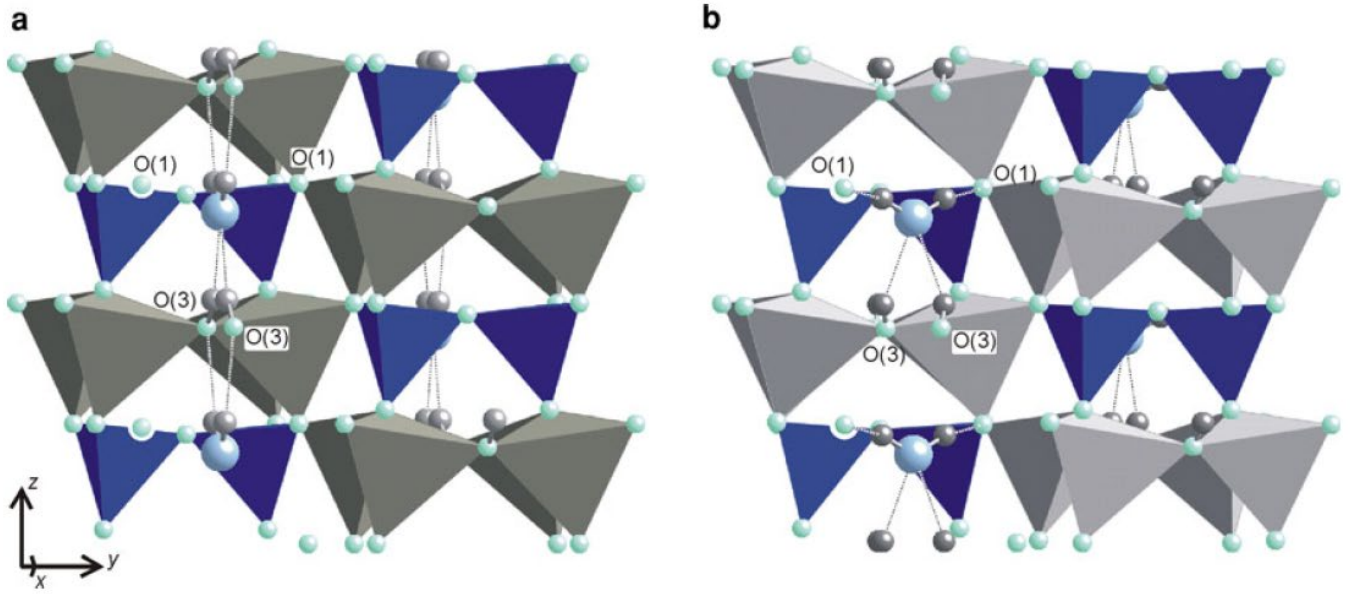

Fig. 5 The configuration of hydrogen bonds in hemimorphite-I (**a**) and in hemimorphite-II (**b**)

Pnn2 at P > 25 kbar **, Seryotkin & Bakakin, *Phys. Chem. Min.* 38 (2011) 679**

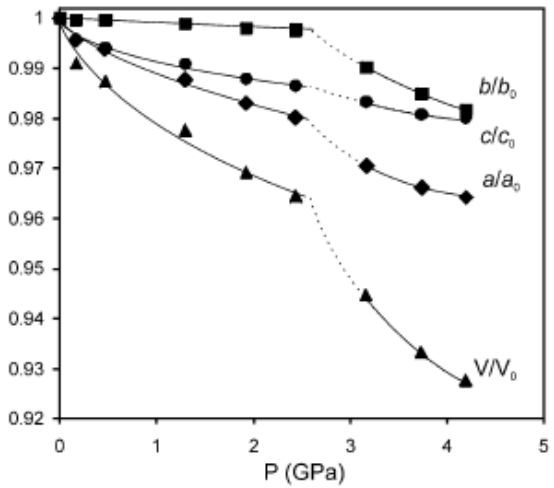

Fig. 1 Evolution of the lattice parameters of hemimorphite under pressure

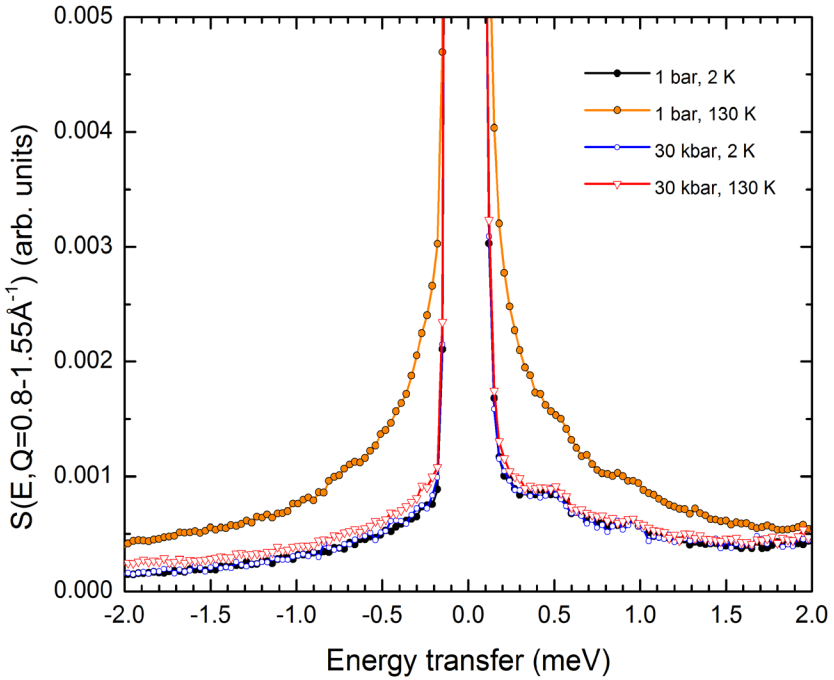

Summary, hemimorphite

- **The QENS data for hemimorphite provide clear evidence that the confined water molecules undergo local diffusive motion even at cryogenic temperatures, T=70-130 K, at which other hydrogen bonded confined water is usually immobile. There are two thermally activated relaxation processes:**
  1) **a faster one on the subpicosecond timescale, and**
  2) **a slower one on the 10-100 ps timescale.**

- **The obtained result on hemimorphite indicates that the origin of the rotational diffusion of water molecule in the crystal at low temperatures is a planar configuration of the hydrogen bonds, which are weak due to strong deformation compared to standard tetrahedral configuration of hydrogen bonds in bulk water.**

OUTLINE

- Introduction
- Fast rotational dynamics of water in hemimorphire
- Dynamics of water in beryl
- Summary

Dom Pedro Aquamarine (Beryl) at the Smithsonian's National Museum of Natural History, Washington D.C.

Hemimorphite, Ojuela Mine, Mapimi, Durango, Mexico

Beryl

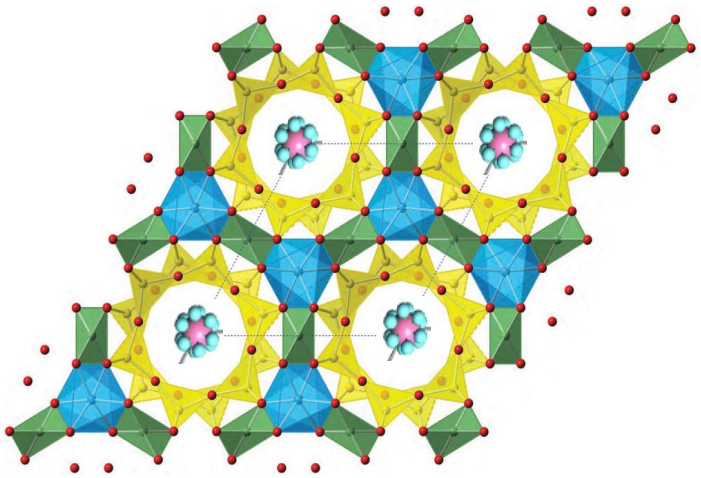

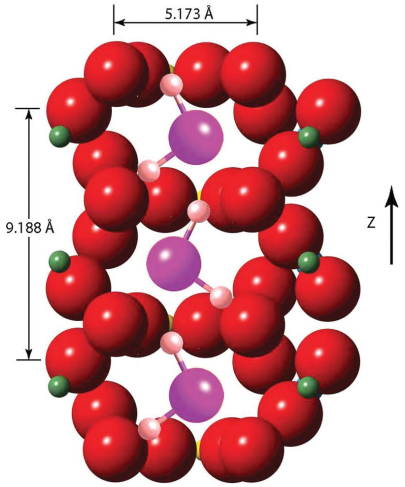

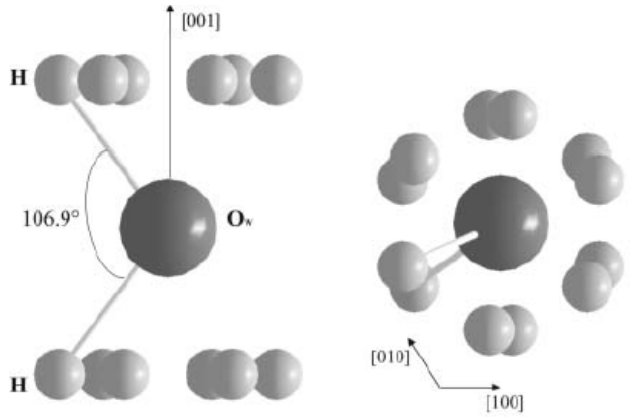

(Left) Structure of beryl ($Be_3Al_2Si_6O_{18}$•$0.6H_2O$, space group *P6/mcc*) showing channels running parallel to the crystallographic *c*-axis (out of the figure's plane): Si, yellow; Al, blue; O, red; and Be, green.

(Middle) Graphical representation of the alignment of water molecules inside the channels, beryl oxygen, red; water oxygen, dark pink; water hydrogen, light pink; beryllium, green; and silicon, yellow.

Topological configuration of water molecules in the channel of the alkali-poor beryl, viewed down [100] (left) and down [001] (right).

G.D. Gatta *et al*. Am. Mineral. 91 (2006) 29

S(Q,E) spectra of beryl, SEQUOIA

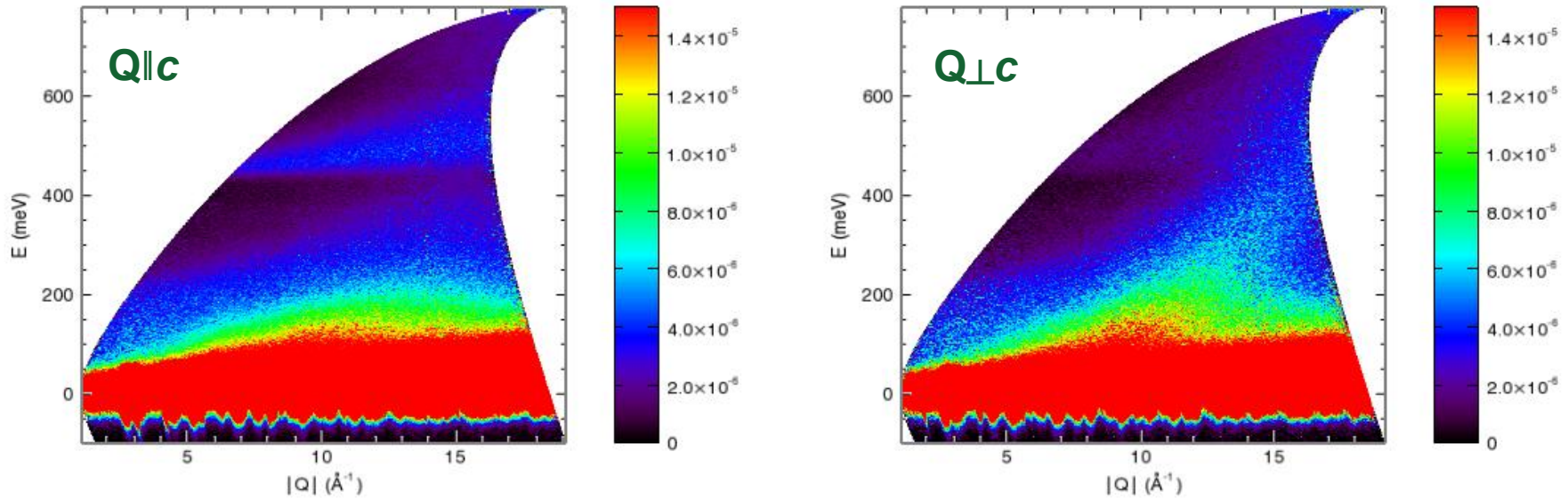

(Q,E) contour plots of S(Q,E) spectra for the neutron momentum transfer Q being perpendicular and parallel to crystallographic *c*-axis. The INS data were collected at T=6 K with E_i=800 meV.

$$S_{1ph}^{inc}(\mathbf{Q},E)=\sum_i \frac{\sigma_i \hbar^2}{6NEM_i}\exp[-(\mathbf{Qu}_i)^2][n_B(E,T)+1]\sum_{j,\mathbf{q}}\left|\mathbf{Qe}_i(j,\mathbf{q})\right|^2,$$

$$(\mathbf{Qu}_i)^2=\int\sum_{j,\mathbf{q}}\frac{\hbar^2}{6NEM_i}|\,\mathbf{Qe}_i(j,\mathbf{q})\,|^2[2n_B(E,T)+1]\delta[E-E(j,\mathbf{q})]dE$$

L.M. Anovitz *et al.*, Phys. Rev. E 88 (2013) 052306
A.I. Kolesnikov *et al.*, J. Phys. Chem. B 118 (2014) 13414

Beryl

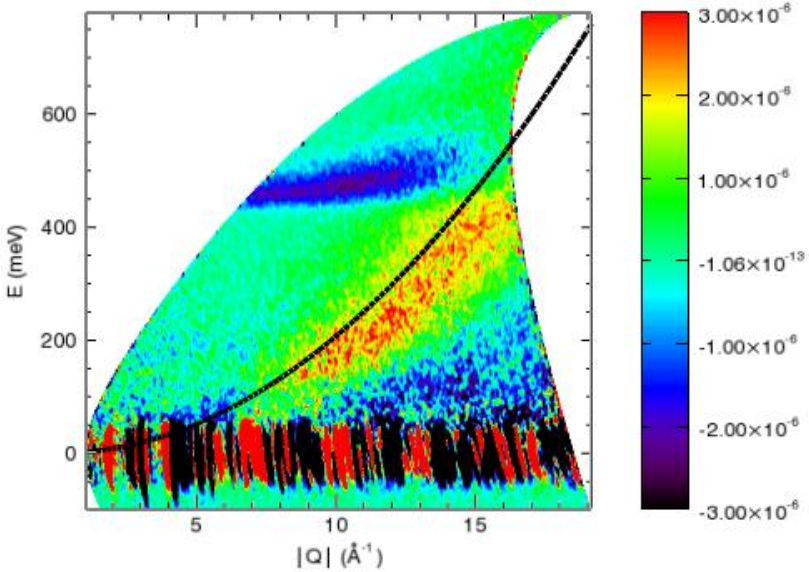

Difference between the S(Q,E) spectra from beryl at 6 K for Q⊥*c* and Q||c orientations. The solid line shows the neutron recoil spectrum for free particle of mass *m*=1 a.u., $E=\hbar^2Q^2/2m$.

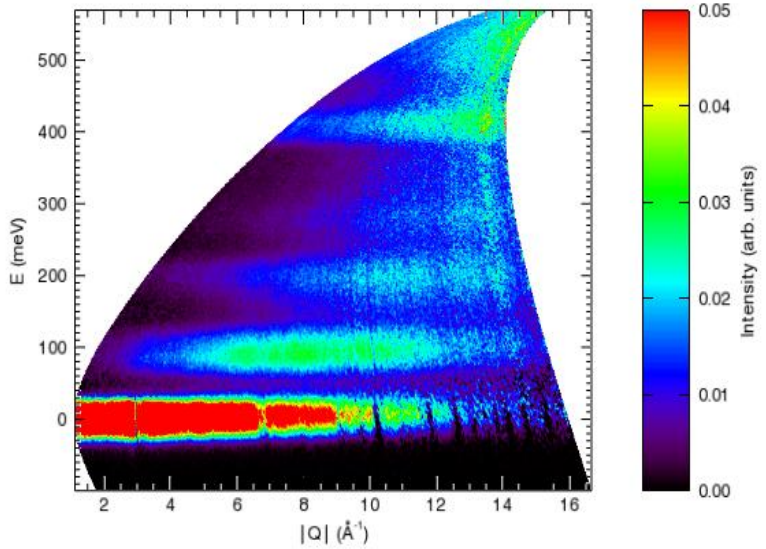

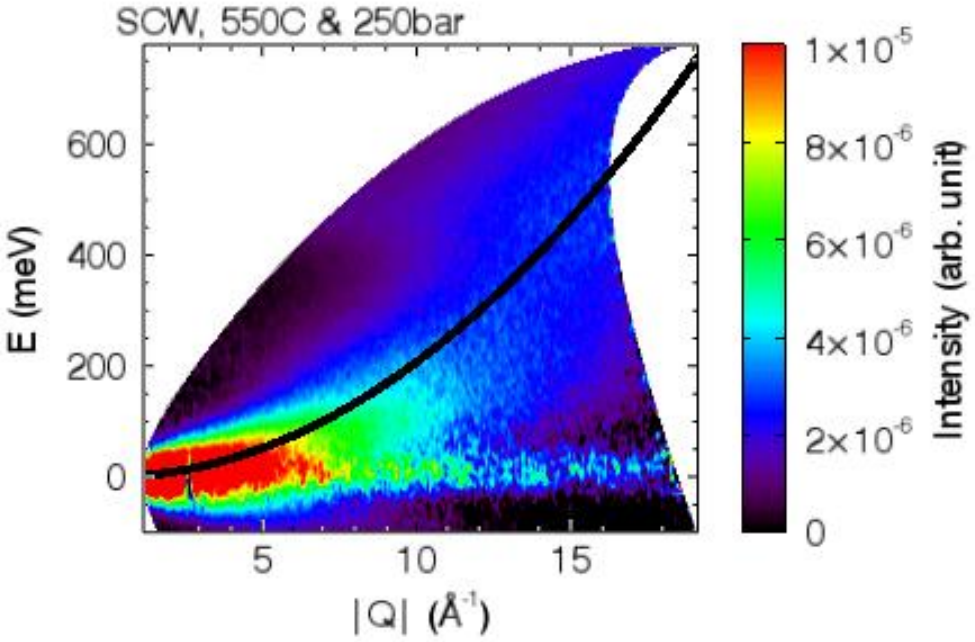

INS spectra of ice-Ih at T=6 K (left) and supercritical water at T=823 K and P=250 bar (top, right).

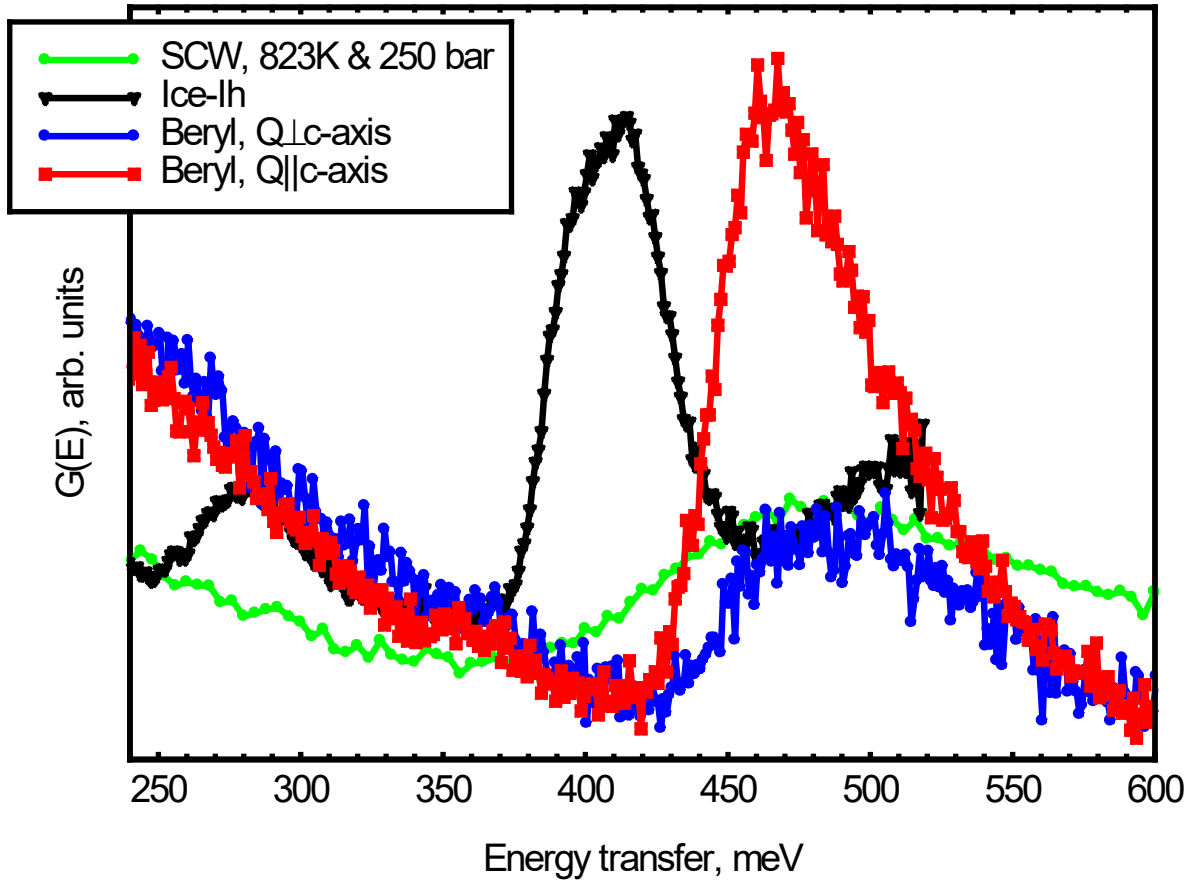

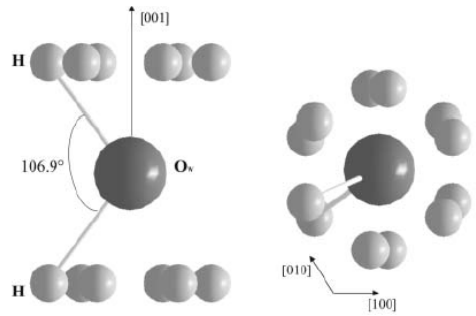

INS spectra at T=6 K for beryl measured with neutron momentum transfer Q parallel and perpendicular to the crystallographic *c*-axis; E_i=800 meV, compared to supercritical water at T=823 K & P=250 bar, and ice-Ih at T=6 K (E_i=600 meV). The confined water intramolecular O-H stretching peak is at 465 meV.

Beryl

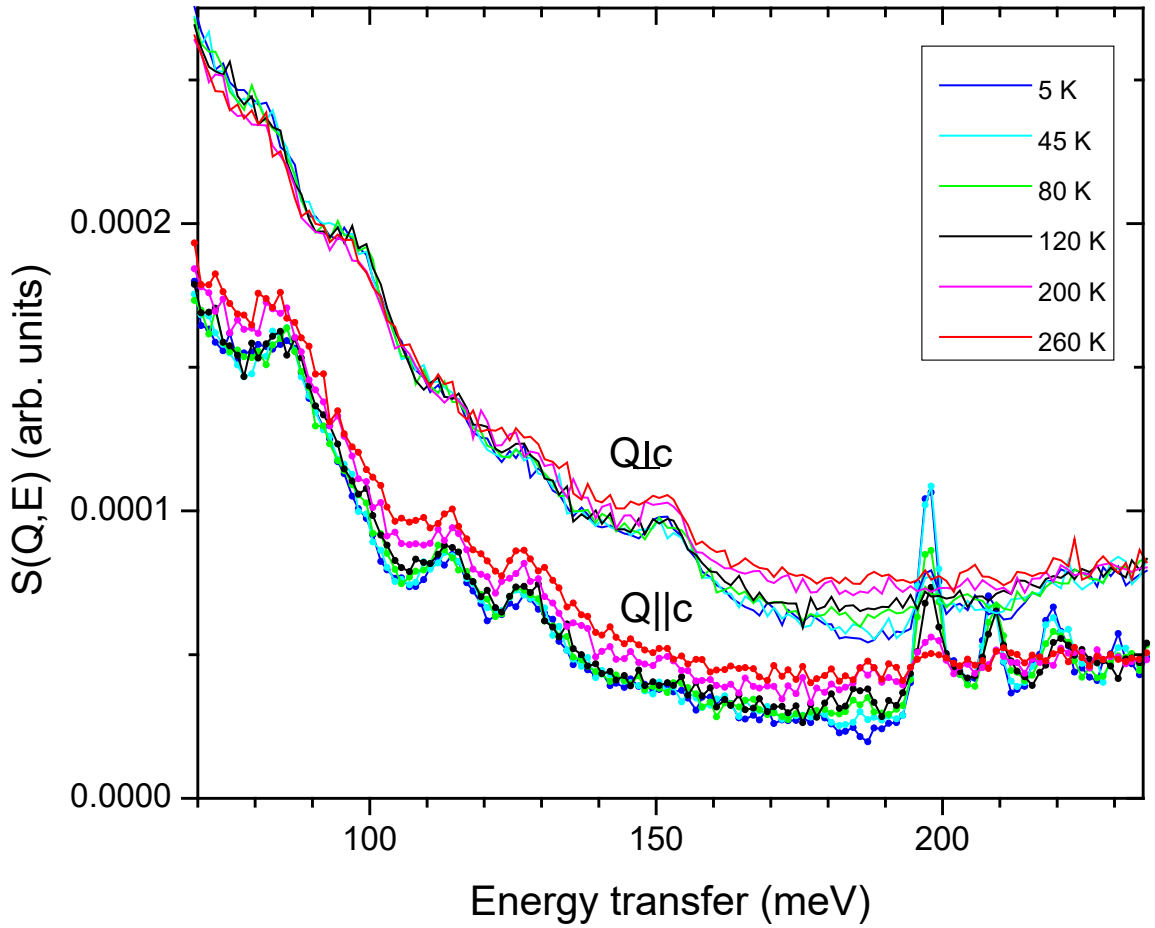

INS spectra for E_i=250 meV. The peak at 197 meV is due to H-O-H bending mode (ν_2), E_{bend}=197.3+0.26(459.7-E_{str}), [1]. Three peaks at the right are due to multi-phonon neutron scattering involving ν_2 and translational modes (~11 meV) of water molecule along the *c*-axis.

[1] M. Falk, Spectrochim. Acta A40 (1984) 43.

Beryl

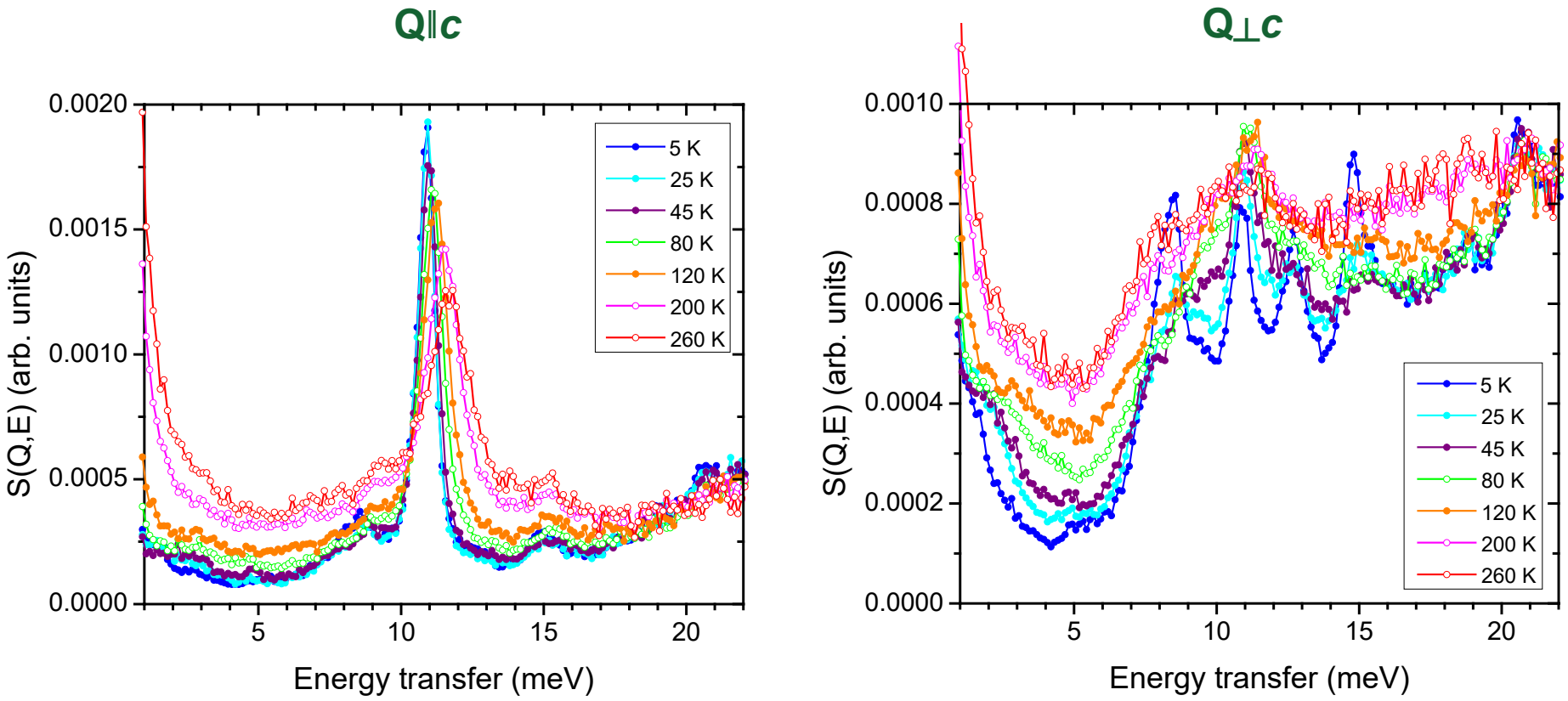

INS spectra of water in beryl, E_i=25 meV, Q parallel and perpendicular to the *c*-axis.

Q∥*c*

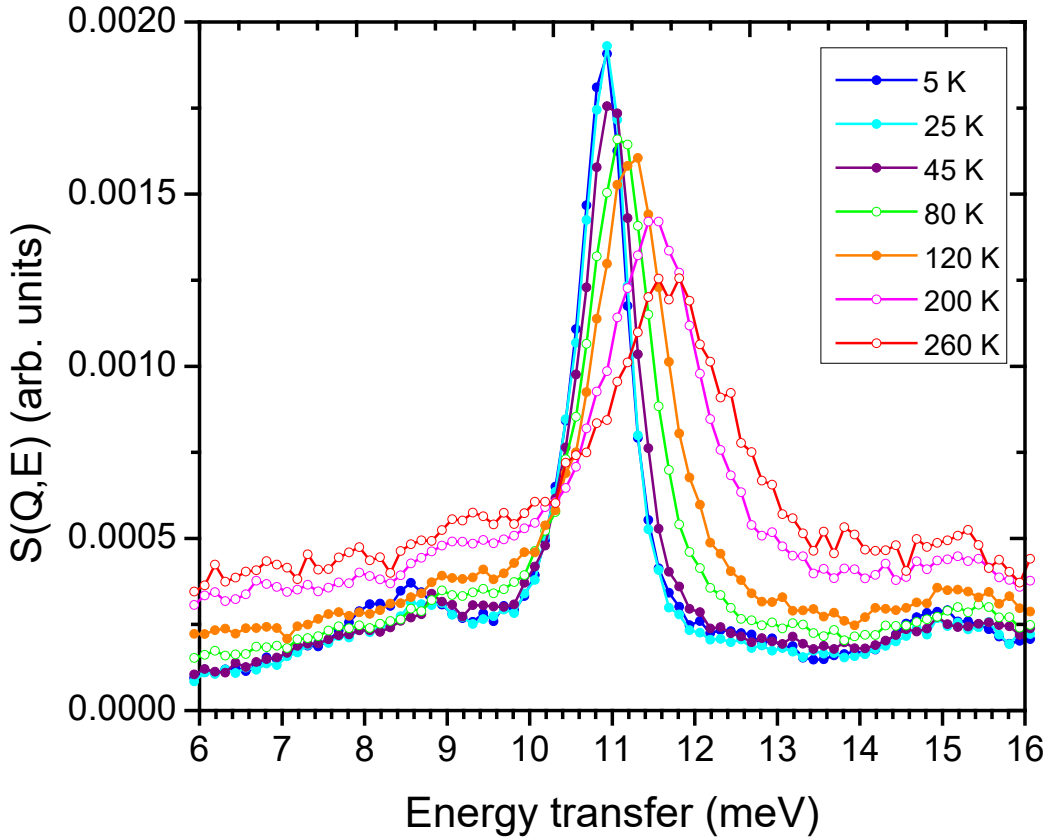

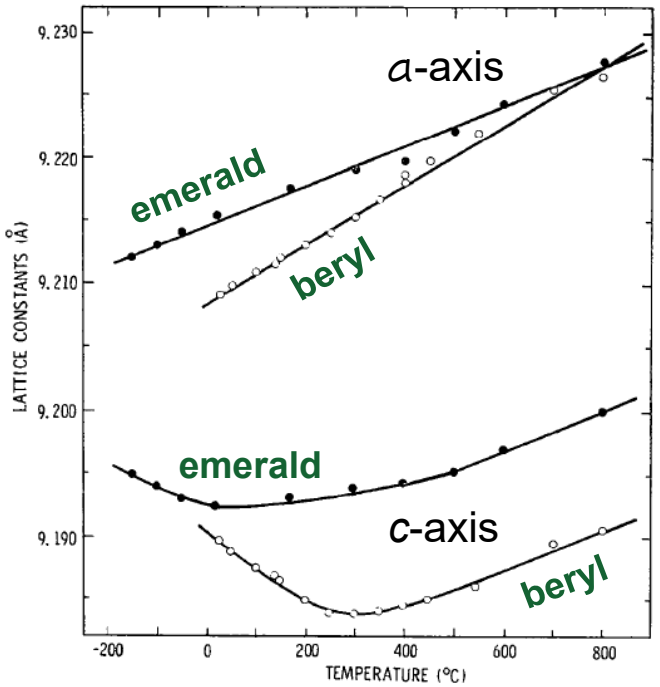

Lattice constants as a function of temperature for beryl and emerald. The values for beryl are shown as open circles, for emerald as solid circles. Note that both crystals exhibit a negative thermal expansion along the *c*-axis. B. Morosin, *Acta Cryst.* B28 (1972) 1899.

Beryl

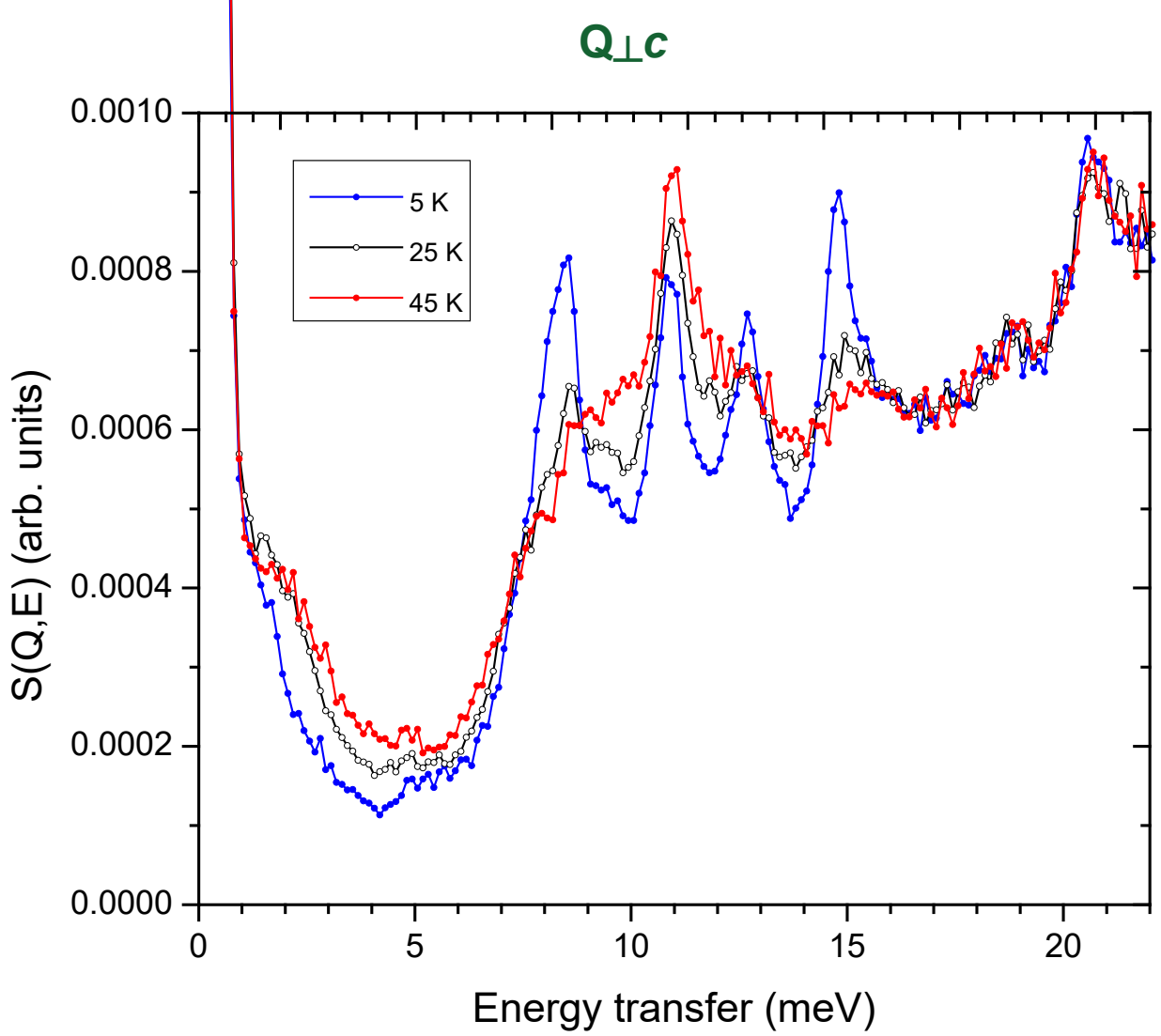

INS spectra of beryl, E_i=25 meV, Q perpendicular to the *c*-axis. The intensity of the peaks at 8.4, 12.7 and 14.7 meV strongly decrease with temperature increase.

Beryl

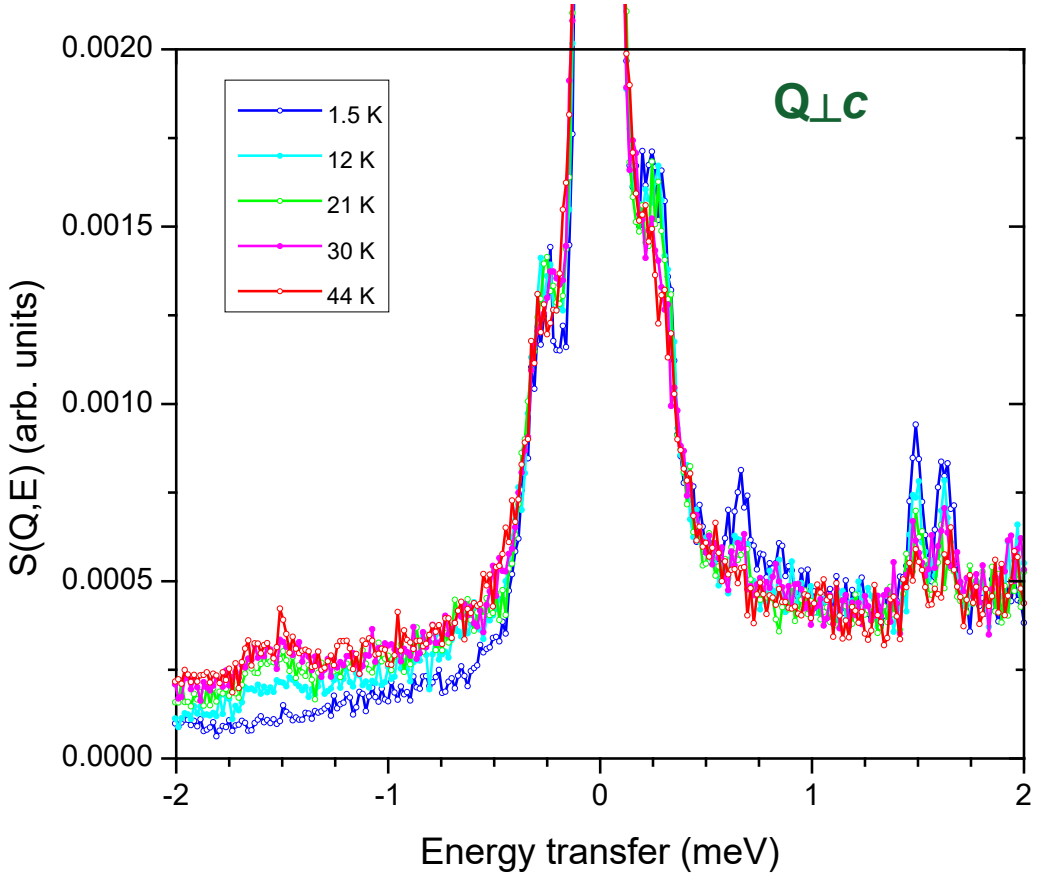

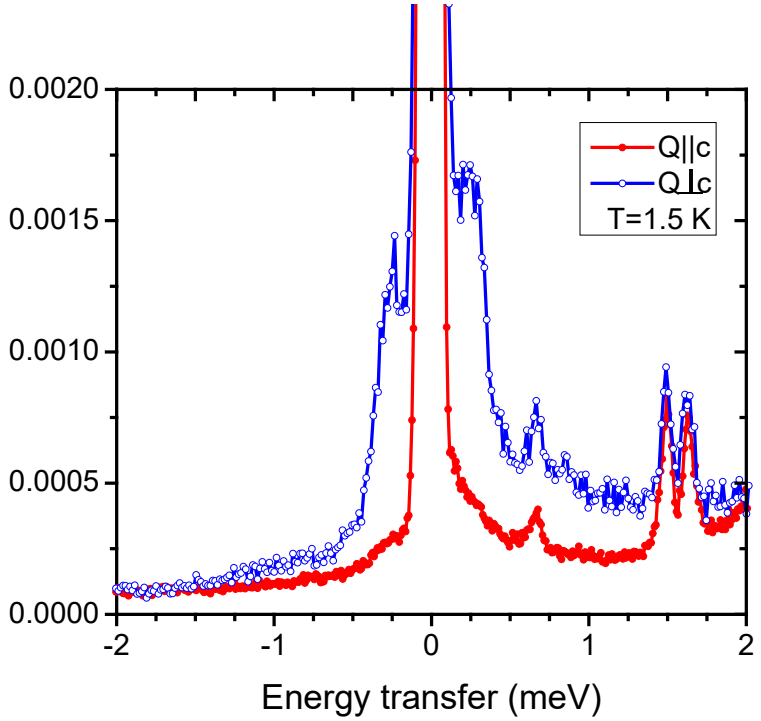

INS spectra of beryl at different temperatures measured with E_i=3 meV at CNCS, Q perpendicular to the *c*-axis (left figure). The intensity of the peaks at 0.27, 0.66, 1.49 and 1.63 meV in energy loss site strongly decrease with temperature increase. The peaks at 0.66, 1.49 and 1.63 meV are isotropic (right figure).

Beryl

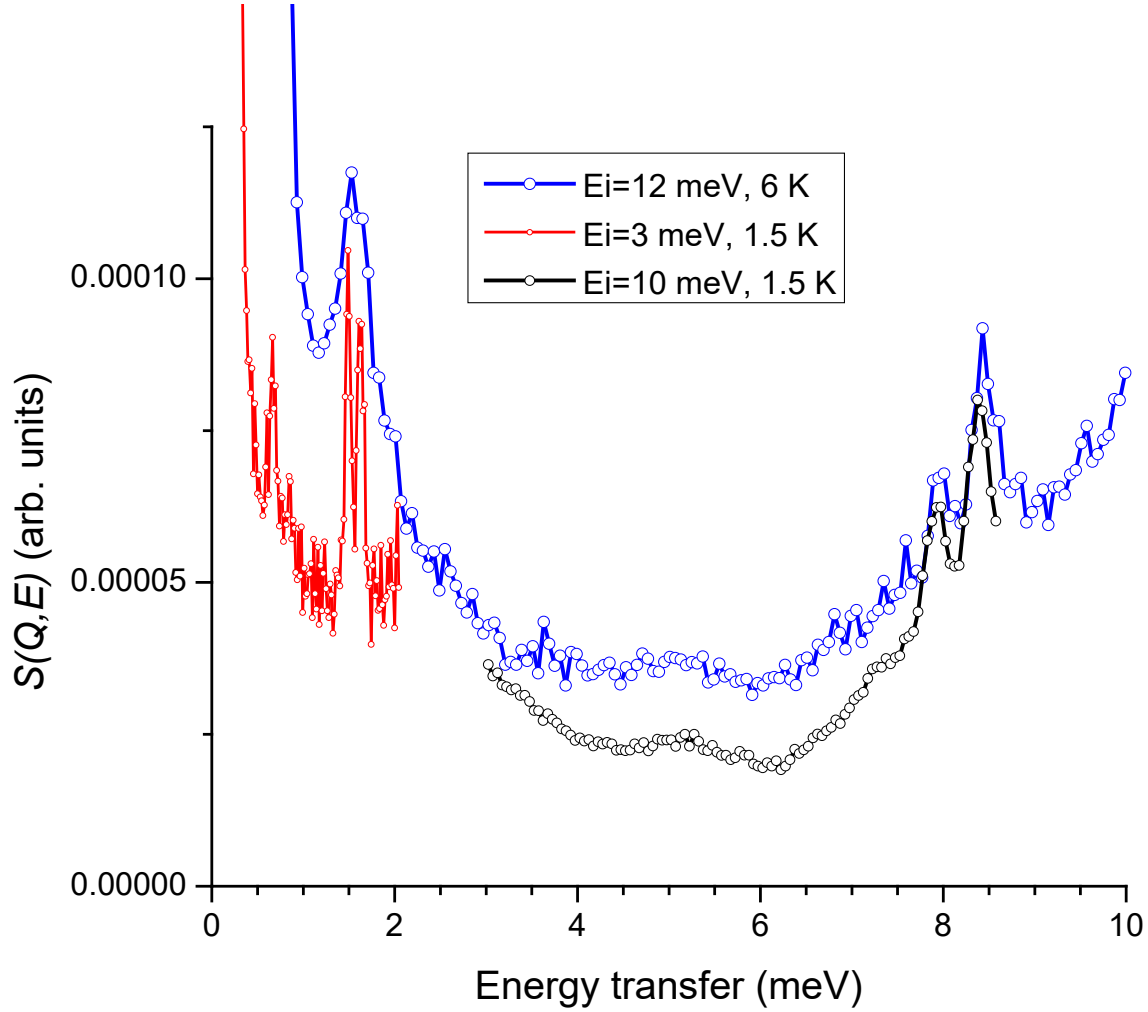

INS spectra of beryl for Q perpendicular to *c*-axis measured at SEQUOIA with E_i=12 meV, and at CNCS with E_i=10 meV, showed that the peak at 8.4 meV is split (7.9 and 8.4 meV).

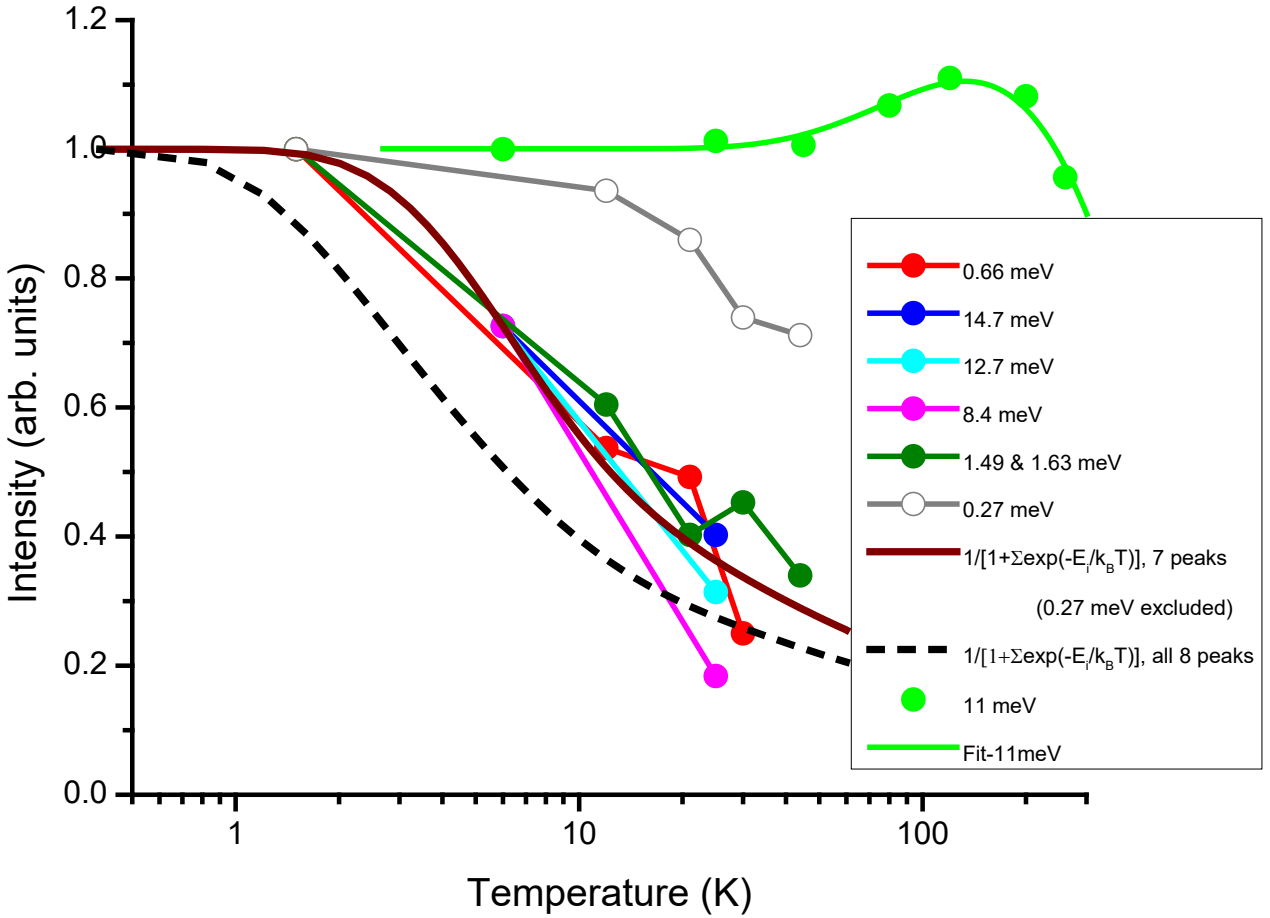

The reduced intensities of the tunneling peaks at energies E_i=0.27, 0.66, 1.49 & 1.63, 7.9 & 8.4, 12.7 and 14.7 meV for Q⊥*c*-axis of beryl (except for the peak at 0.27 meV) follow the temperature dependence for transitions from the lower to higher split ground states, $\mathrm{I(T)} \propto 1/\left\{1+\sum_{i=1}^{7} exp(-\frac{E_i}{k_B T})\right\}$. The intensity of the translational (vibrational) mode at 11 meV (Q||*c*-axis) is shown for comparison. The peaks' intensities are normalized to be 1 at T=0 K.

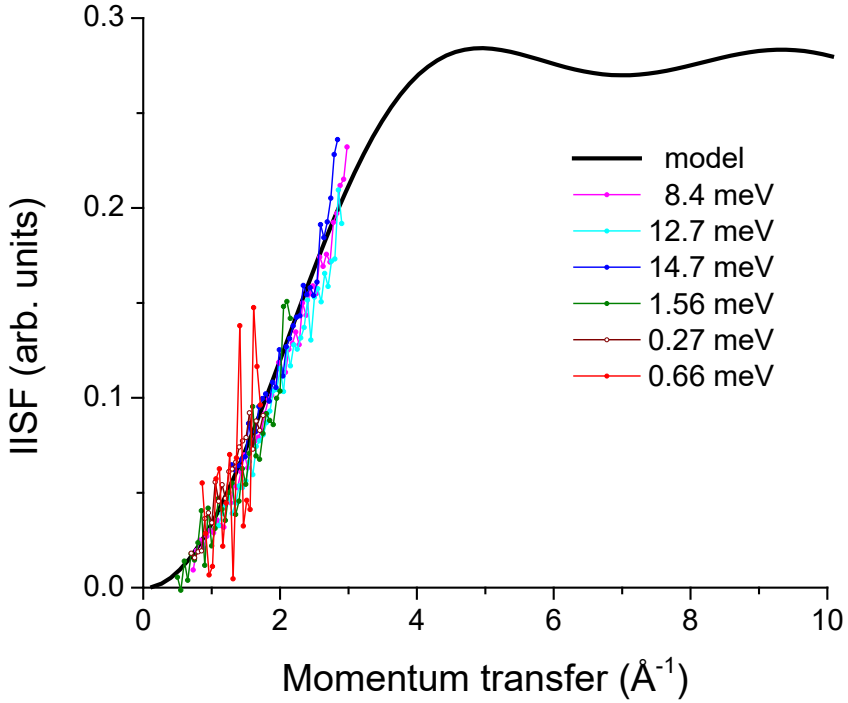

The inelastic incoherent structure factor in INS spectra for particle jumping over $2\pi l/6$ positions on circle of radius d [1]

$$IISF(Q) \propto \frac{1}{6\pi}\sum_{l=1}^{5}\sum_{k=1}^{6} j_0\left(2Qd\,sin\frac{\pi k}{6}\right)\cos\left(\frac{2\pi lk}{6}\right)$$

[1] J.D. Barnes, *J. Chem. Phys*. 58 (1973) 5193

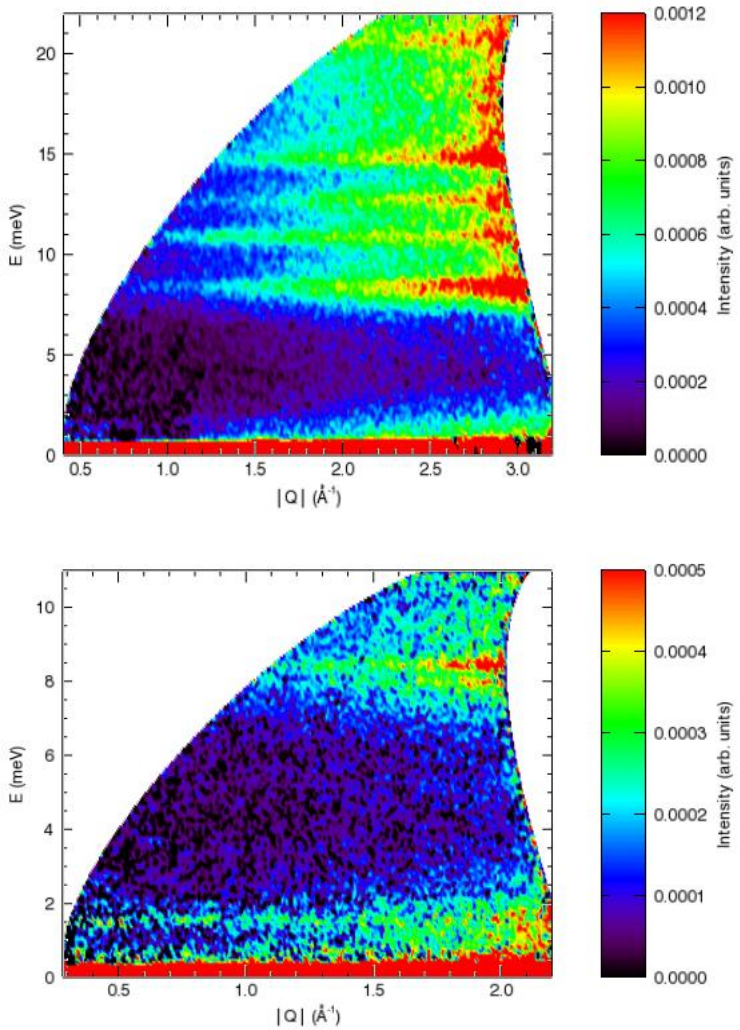

(Q,*E*) contour plots of *S*(Q,*E*) spectrum for beryl at 5 K for Q⊥*c*-axis, E_i=25 meV (top) and 12 meV (bottom), *T*=5 K. The increase of the peaks intensity with Q increase shows that these peaks are not due to magnetic crystal field effect.

Deep Inelastic Neutron Scattering (VESUVIO, ISIS, RAL)

The momentum distribution $n(\mathrm{p})$ of the particles can be measured by Deep Inelastic Neutron Scattering (DINS). DINS is inelastic neutron scattering in the limit of large momentum transfer, Q (~30-100 Å^{-1}). $S(\mathrm{Q}, E)$ in this limit takes the form:

$$S(\mathrm{Q}, E) = \int n(\mathrm{p}) \delta \left(E - \frac{\hbar^2 \mathrm{Q}^2}{2M} - \frac{\hbar \mathrm{Q} \mathrm{p}}{M} \right) d\mathrm{p}$$

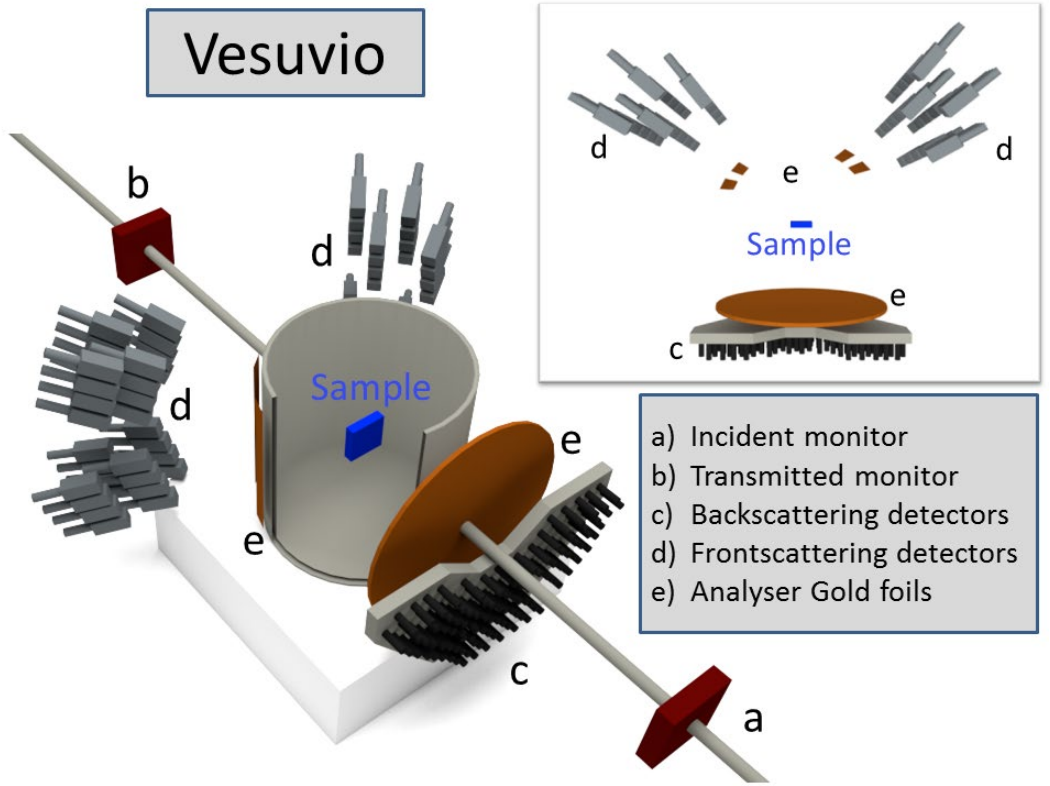

Analyzing energy: 4906 meV (Au)

DINS measurements were done at 4.3 K for two crystal orientations of beryl, with *c*-axis along and perpendicular to the incoming neutrons. The spectra were transferred to the 3D momentum distribution of water protons in beryl *n(p)* by simultaneous fit of all data using the Hermite polynomials of the 8 order (George Reiter, Un. Houston, TX).

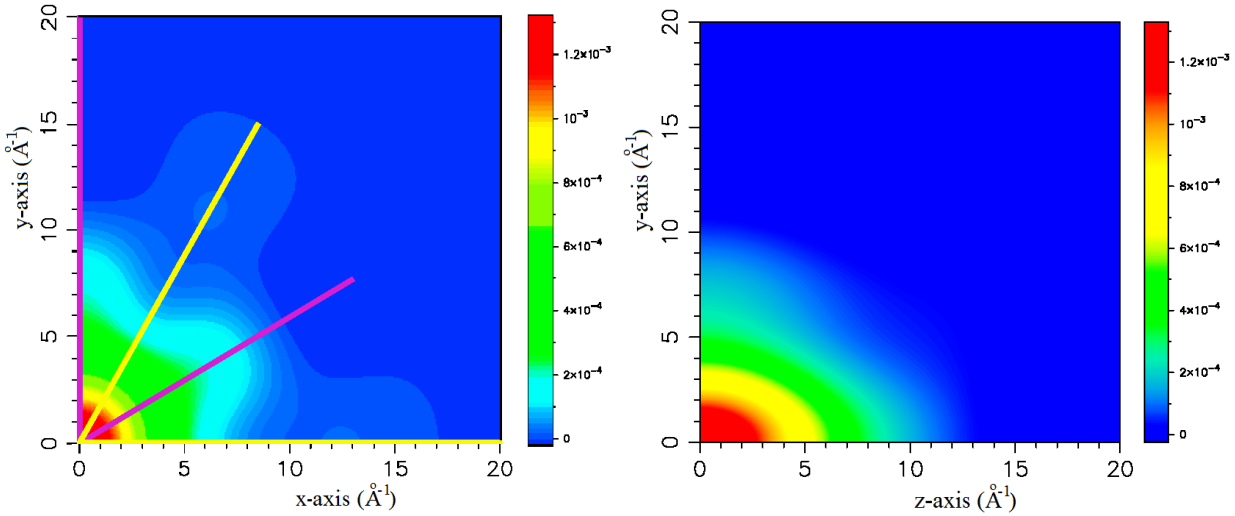

Projection of water proton momentum distribution *n*(p) onto the *xy*- and *yz*-planes.

The values of *n(p)* broadening are: σ_x=3.66, σ_y=3.61 and σ_z=4.98 Å^{-1}, therefore the kinetic energy of the proton, $\langle E_K \rangle = \frac{\hbar^2}{2M}\left(\sigma_x^2 + \sigma_y^2 + \sigma_z^2\right)$=106 meV, is much smaller than has been observed in bulk water (~150 meV).

The water proton kinetic energy can be estimated by using semi-empirical approach in quasi-harmonic approximation (Moreh and Nemirovsky, *J. Chem. Phys.* 133 (2010) 084506)

$$E_K = S_t \int_0^{v_t} \alpha_t g_t(v)dv + S_r \int_{v_{r1}}^{v_{r2}} \alpha_r g_r(v)dv + \sum_{j=1}^{3} S_j \frac{1}{2}\alpha_j ; \quad \alpha_i = \left(\frac{hv_i}{e^{hv_i/kT}-1} + \frac{hv_i}{2}\right)$$

and *S* is the kinetic energy fraction for water proton, which for intramolecular vibrations is about 0.47, for librational modes S_r≈0.475, and for translational vibrations $S_t=M_H/M_{H2O}$=1/18. In the case of beryl, using only the intramolecular vibrations of water obtained from INS spectra ($v_1 = v_3 = 465$ meV, and $v_2 = 197.5$ meV) and omitting the translational and librational vibrations of water the estimated E_K = 0.47×(2×465/2 + 197.5/2)/2 = 133 meV, which is larger, than the observed (DINS) experimental value, E_K=106 meV.

Summary, beryl

- **INS spectra of beryl at low temperature show 8 peaks at energies 0.25–15 meV, and the intensity of these peaks strongly decreases with increasing temperature. The data can be explained by transitions between the split ground states of confined water due to it tunneling between the 6-fold equivalent positions across the crystal channels.**

- **DINS data show that water protons exhibit 6-fold momentum distribution across the beryl channel, with additional maxima due to proton coherent delocalization (tunneling). The obtained proton kinetic energy, E_K=106 meV, is much smaller than in bulk water (~150 meV), despite the observed highest O-H stretching modes.**

Acknowledgements

Larry Anovitz	ORNL
George Ehlers	ORNL
Christina Hoffmann	ORNL
Stephan Irle	ORNL
Paul Kent	ORNL
Eugene Mamontov	ORNL
Andrey Podlesnyak	ORNL
Xiaoping Wang	ORNL
Dave Wesolowski	ORNL
Narayani Choudhury	Un. Washington, Bothell, WA
Tim Prisk	NIST, MD
George Reiter	Un. Houston, TX
Andrew Seel	Un. Oxford, UK